Dynamics of granular avalanches caused by local perturbations

Thorsten Emig
Institut für Theoretische Physik, Universität zu Köln, Zülpicher Straße 77, D-50937 Köln, Germany

Philippe Claudin
Laboratoire de Physique et Mécanique des Milieux Hétérogènes, ESPCI, 10 rue Vauquelin, 75231 Paris Cedex 05, France.

Jean-Philippe Bouchaud
Service de Physique de l'État Condensé, Centre d'études de Saclay Orme des Merisiers, 91191 Gif-sur-Yvette Cedex, France

(Dated: February 2, 2008)

Surface flow of granular material is investigated within a continuum approach in two dimensions. The dynamics is described by a non-linear coupling between the two 'states' of the granular material: a mobile layer and a static bed. Following previous studies, we use mass and momentum conservation to derive St-Venant like equations for the evolution of the thickness R of the mobile layer and the profile Z of the static bed. This approach allows the rheology in the flowing layer to be specified independently, and we consider in details the two following models: a constant plug flow and a linear velocity profile. We study and compare these models for non-stationary avalanches triggered by a localized amount of mobile grains on a static bed of constant slope. We solve analytically the non-linear dynamical equations by the method of characteristics. This enables us to investigate the temporal evolution of the avalanche size, amplitude and shape as a function of model parameters and initial conditions. In particular, we can compute their large time behavior as well as the condition for the formation of shocks.

PACS numbers: 45.70.Ht — Avalanches, 45.70.-n — Granular systems, 05.45.-a — Nonlinear dynamics and nonlinear dynamical systems

I. INTRODUCTION

The dynamics of granular avalanches has been keeping busy a large fraction of the granular community for several years. As an example, a recent review paper has been written by the French research group named 'GdR Milieux Divisés' in order to sum up the 'French results' of experiments and numerical simulations on steady uniform dense granular flows [1]. Some of the recurring issues addressed in this long article concern the definition and the description of the rheology and the friction law of these flows. As a matter of fact, these quantities are important physical ingredients to be plugged into the equations proposed for the modeling of these avalanches. Although some alternative models are proposed – see e.g. [2, 3] – an interesting theoretical framework for the description of granular flows follows the St Venant-like approach for thin flows in hydrodynamics, in which conservation equations are integrated over the depth of the flow [4]. This was proposed for example by Savage, Hutter and co-workers for the case of the motion of grains over an inclined rough plane [5].

With such equations adjusted on uniform steady flows, it is for instance possible to reproduce quantitatively steady fronts of granular avalanches on a rough inclined plane [6]. Another interesting situation is that of unsteady avalanches, whose dynamics is of course more complicated to capture and is very demanding for the models. An example of such a situation is the motion of an initially confined granular mass which is released and runs down the same rough plane. In this case, the same calibration gives also quite good qualitative predictions [7]. The spreading of a granular mass is also of interest in a geophysical context as they are a model of real cliff collapse [8, 9]. Another famous example is the case where an initial static layer of grains is available on the plane, and avalanches triggered by a local solicitation with a pointy object [10, 11]. The nice experimental pictures show two types of behavior: a 'triangular avalanche' when the thickness of the grain layer is small, and an avalanche with an 'up-hill' propagative front when the layer is thicker.

In the present paper, our aim is also to deal with unsteady and non-uniform granular flows in a geometry close to these elementary 'response' situations where avalanches are caused by local perturbations. More precisely, we look at the dynamical evolution of a uniform slope on which some amount of rolling grains is initially deposited locally. However, unlike the above examples, we shall focus on avalanches running over an erodible bed, i.e. an infinite grain layer for which the selected thickness of moving grains is not fixed *a priori* or bounded by a plane. This situation then has one extra dynamical degree of freedom. As will be made more precise in the next section, in order to close

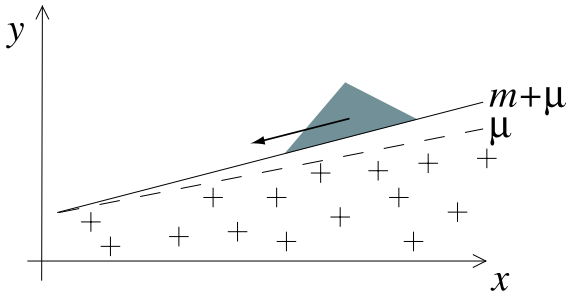

FIG. 1: Rolling grains are locally deposited on a static sand bed which has initially a uniform slope $\mu + m$, where μ is the tangent of the angle of repose.

these equations it is indeed necessary to specify the shape of the velocity profile of the moving grains and to explicit the different forces acting on them. Moreover, as our theoretical work aims at obtaining exact results on avalanche profiles, the analysis will be restricted to two dimensional systems for simplicity, and will be relevant for experiments in confined cells or when the perturbation has translation invariance in the direction perpendicular to the slope.

General St Venant equations for granular avalanches on erodible beds have been recently proposed by Douady *et al.* in [12]. Observations show that these avalanches consist of a thin moving layer of grains over a (quasi)static profile [13]. The two natural variables in this modeling are therefore the profile of the static pile Z, and the thickness of rolling grain layer R that flow over this bed, both functions of time and horizontal position. In this framework, we shall derive two particular sets of coupled equations for R and Z that are simple enough to be solved exactly for the 'response geometry' described above. As will be explicited in the next section, they are based on different choices for the velocity profile in the flowing grain layer, and exhibit different non-linearities. A particular case of one of the two studied sets gives in fact the equations proposed in [14] on more phenomenological grounds, and for which we developed an analytical treatment in [15] using the method of characteristics. We extend here this powerful technique to all other cases as well. This technique has been also applied to a St Venant like model for debris avalanches [16].

After the derivation of these sets of equations in section II in which we shall specify the assumptions made, both sets of equations – corresponding to different flow profiles – are treated in the following two sections. We show the different predictions of the models, compare how the triggered avalanche dies out or grows depending whether the initial slope of the static profile is smaller or larger than the repose angle of the pile, and discuss the appearance of shocks. We finally conclude and draw perspectives on the description of avalanche fronts. The present paper is rather technical, but we hope that the scope of the method used is sufficiently broad to warrant interest in itself; furthermore, obtaining explicit exact result for the shape of avalanche shapes and sizes gives important benchmarks to which experiments can be compared, and will eventually help selecting the correct set of hydrodynamical equations for granular avalanches.

II. ST VENANT EQUATIONS FOR GRANULAR AVALANCHES

The aim of this section is to (re-)establish coupled differential equations for the variables R and Z introduced above and depicted in figure 2. These equations encode the conservation of the number of grains as well as their horizontal momentum [12]. They describe how static grains may be dislodged and contribute to the flow (erosion), and vice-versa how moving grains may come to rest (deposition) [14].

Besides R and Z, another important field is of course the velocity in the moving layer. Let us note $u(x, y)$ the horizontal component of the velocity profile in this layer – although not explicited, time dependence of u is understood. The averaged velocity of the flow can be defined as $U = \frac{1}{R}\int_Z^{Z+R} dy\, u(x, y)$. With this quantity, the number of particles passing through a vertical line in x during the time interval dt is $\frac{\rho}{m} RU dt$, where ρ is the mass density of the granular material and m the mass of a single grain. The difference of this number in x and $x + dx$ makes the volume $(R + Z)dx$ change, so that the conservation of matter reads

$$\partial_t(R + Z) = \partial_x(RU). \tag{1}$$

In a similar way, the x-component of the momentum passing through the vertical line in x during dt is $\rho RW dt$, where W is the average of the square of the velocity: $W = \frac{1}{R}\int_Z^{Z+R} dy\, u^2(x, y)$. The change of horizontal momentum $\rho RU dx$

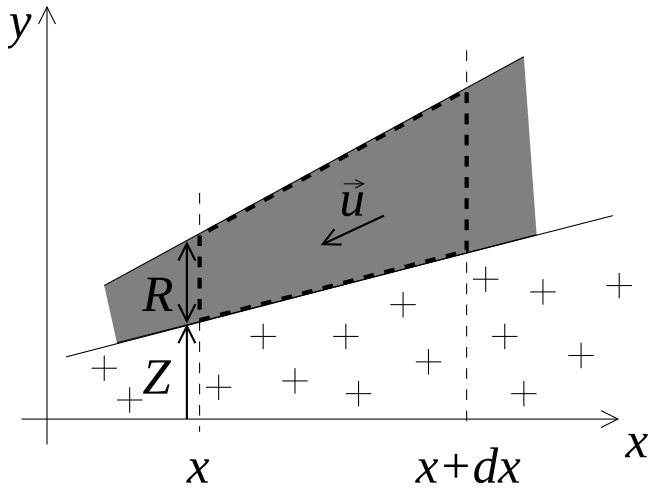

FIG. 2: Rolling phase $R(t,x)$ (grey) and static phase $Z(t,x)$ (crosses). The grains flow from the right to the left. The dashed box is the control volume for which mass and momentum conservation laws are written.

in the control volume (see figure 2) can then be written as

$$\partial_t(RU)\,dx = \partial_x(RW)\,dx + \frac{1}{\rho}\,dF_x, \tag{2}$$

where dF_x is the $x-$component of the forces acting of this volume.

These forces are of two kinds: those coming from the lateral sides through the stress σ_{xx}, and those due to the contact between the rolling and the static phase. Assuming a horizontal normal stress proportional to the 'hydrostatic' pressure $\sigma_{xx}(x,y) = b\,\rho g(R+Z-y)$, the corresponding force is $\int_Z^{Z+R} dy\,\sigma_{xx} = \frac{1}{2}b\rho g R^2$. Numerical simulations suggest values for b that increase from roughly one half in static piling to unity for uniform steady flows [1, 17, 18]. In [5] the value of b is obtain for unsteady and inhomogeneous situations from a Mohr-Coulomb yield criterion. It turns out that b can increase (decrease) compared to unity if the grains are compressed (decompressed) by the flow. Here we consider b as a phenomenological *constant*. Taking the difference of this force on the two sides of the control volume, the contribution of the horizontal normal stress to dF_x finally reads $b\rho g R\partial_x R\,dx$. To compute the other part of dF_x, we assume that the grains in the control volume behave, with respect to the static phase, like a frictional solid (with normal reaction N and friction force T). We call μ the friction coefficient. Defining θ by $\tan\theta = \partial_x Z$, the balance of the weight of this volume gives $\rho g R\,dx = N\cos\theta + T\sin\theta$. With $T = \mu N$, the horizontal contribution of N and T to dF_x (to the lowest order in θ and μ) is $\rho g R(\partial_x Z - \mu)\,dx$. In summary, we get

$$dF_x = b\rho g R\partial_x R\,dx + \rho g R(\partial_x Z - \mu)\,dx. \tag{3}$$

Several remarks are in order at this point. First of all, we have assumed that the granular density ρ is the same in the moving and the static parts, which is certainly a valid hypothesis for dense flows as considered here. More importantly, the friction coefficient μ will be taken as a constant in the following. It is however well established that there are few degrees of hysteresis between the starting and the stopping angles, which can be simply understood even at the scale of a single grain rolling down a "pile" consisting of a layer of regularly spaced fixed grains [19]. As will be emphasized in the conclusion, this slight difference is of great importance when it comes to the description of regions where the moving layer is about to jam or the static bed about to move, i.e. at the feet of avalanche fronts ($R \to 0$). Besides, it has been shown that in quasi 2D experiments conducted in a thin channel between two plates, the friction of the rolling on those plates plays a major role in the dynamics of the avalanche [20, 21]. Such a boundary effect is not encoded here.

Finally, these equations will be closed by making an explicit choice for the velocity profile u. The integrals for the computation of U and W will then be expressed as a function of R. This means that we implicitly assume *instantaneous* adaptation of the velocity to the flow. In principle, like R and Z, the averaged velocity U is an independent dynamical variable whose dynamics should be described by an additional equation of 'internal force balance' $\partial_t U = \ldots$. The right hand side would specify the part of the forces acting on the moving layer that contribute to the acceleration and friction of the rolling grains rather than the erosion/deposition processes, i.e., the exchange between R and Z. A model similar to our Eqs. (1) - (3) has been very recently studied by Khakhar et al. [22] but for different geometries and

initial conditions (heap and rotating cylinder flows). Their momentum balance equation has however an additional term which describes grain collisions in the mobile phase. Thus they combine effects of internal dissipation [23] and external forces as gravity and solid like friction between the two phases.

Two choices for the velocity profile will be investigated below: the plug flow for which $u(x,y) = U = \text{Cst}$ (named model $\mathcal{P}$ for 'plug'), and the situation with a linear velocity profile $u(x,y) = \gamma y$ (named model $\mathcal{L}$ for 'linear'). The natural selection of this profile is still a puzzling issue and is the result of several mechanisms at the grain level (e.g. trapping) or at larger scales (non-local effects, clustering) [24, 25]. At the phenomenological level, the first case is reasonable for the description of thin or dilute flows (when R of the order of a grain diameter) [26], and the second one is strongly supported by experiments and simulations performed on *steady and deep* 2D systems [1]. In particular, it should be emphasized that the velocity gradient is found to be constant, and it is the thickness of the rolling layer R which adapts its value to the external imposed shear stress, see e.g. [1, 27]. In contrast, note that for steady granular flows on a fixed rough inclined plane a Bagnold-like velocity profile $U \propto R^{3/2}$ is observed. For the study of unsteady situations, since the static profile Z is now specified, the two St Venant conservation equations can be used for the determination of the space and time evolution of R and U [7].

III. PLUG FLOW: CONSTANT VELOCITY PROFILE (MODEL $\mathcal{P}$)

For a plug flow with a constant average horizontal velocity U we trivially get $W = U^2$, and one obtains from the analysis in section II the model

$$\partial_t Z = -R\,\partial_x Z - b\,R\,\partial_x R, \tag{4a}$$
$$\partial_t R = \partial_x R + R\,\partial_x Z + b\,R\,\partial_x R. \tag{4b}$$

Here the dimensionless t, x, R and Z are measured in units of U^2/g, and t is rescaled by U/g. Furthermore, as we are interested in surface profiles close to the avalanche slope μ, Z is measured relative to the critical slope, i.e., it is replaced by $Z + \mu x$. The quantity b is then the only free parameter of these equations. Recall that an isotropic stress distribution corresponds to $b = 1$. Note also that setting $b = 0$ yields the so-called BCRE model introduced in [14] (although without the diffusive terms considered there). Any small but finite b thus leads to novel non-linearities. Before we study the propagation of a localized perturbation, as a first simple benchmark of the model, we briefly note the predictions of the model for the initial situation of a constant slope $Z_0(x) = mx$ and a homogeneous amount of rolling grains, $R_0(x) = \varrho$. It is easy to see that in this case the thickness of the mobile layer growths (or decays) exponentially in time, depending on the sign of m, with $R(t,x) = \varrho e^{mt}$. The static profile is then given by $Z(t,x) = mx + \varrho(1 - e^{mt})$. Note that this solution does *not* depend on b since $R(t,x)$ is independent of x.

A. Infinite stress anisotropy ($b = 0$)

1. *Analytical solution*

This non-linear model has been studied previously for the case of a static profile consisting of two regions of constant but different slopes and an initially homogeneous (constant) amount of rolling grains [15]. However, the method of characteristic curves can be also employed to study local perturbations in form of an initially localized amount $R_0(x)$ of rolling grains. In fact, for arbitrary initial profiles $R_0(x)$ and $Z_0(x)$ the solution of equations (4) with $b = 0$ can be obtained analytically in implicit form. Using the method of characteristic curves, see Appendix A, we introduce the new coordinates $\alpha(t,x)$ and $\beta(t,x)$. The mapping between the two coordinate systems depends on the solution for $R(t,x)$, $Z(t,x)$ and thus on the initial profiles due to the non-linearities. The so-called characteristic equations, which determine simultaneously the coordinate mapping and the profiles, for this model read

$$\partial_\alpha x - \zeta_+ \partial_\alpha t = 0, \tag{5a}$$
$$\partial_\beta x - \zeta_- \partial_\beta t = 0, \tag{5b}$$
$$-R\partial_\alpha Z + (\zeta_+ - R)\,\partial_\alpha R = 0, \tag{5c}$$
$$-R\partial_\beta Z + (\zeta_- - R)\,\partial_\beta R = 0, \tag{5d}$$

with the characteristic directions given by

$$\zeta_+ = -1, \quad \zeta_- = R. \tag{6}$$

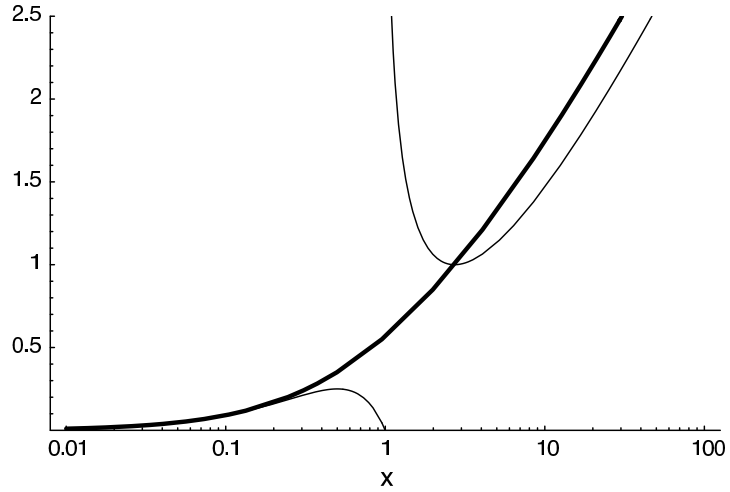

FIG. 3: Bold curve: plot of the Lambert's function $W(x)$. Thin curves: small and large x expansions $W(x) \sim x - x^2$ and $W(x) \sim \ln x - \ln\ln x$, respectively.

The solution of these equations can be obtained explicitly,

$$t(\alpha,\beta) = -\int_{-\alpha}^{\beta} \frac{d\beta'}{1+R(\alpha,\beta')} \tag{7a}$$

$$x(\alpha,\beta) = -\beta - t(\alpha,\beta). \tag{7b}$$

As function of these new coordinates the solution can be written in the closed form

$$Z(\alpha,\beta) = Z_0(\alpha) \tag{8a}$$

$$R(\alpha,\beta) = W\left[R_0(-\beta)e^{R_0(-\beta)+Z_0(-\beta)-Z_0(\alpha)}\right], \tag{8b}$$

where W is Lambert's function [28], see Fig. 3. Before we proceed with special choices for localized initial profiles $R_0(x)$, we would like to point out that the model of equations (4) with $b = 0$ can be still solved exactly if the coefficient of $\partial_x Z$ on the right hand side of both equations is a general function of $R(t,x)$, $\mathcal{F}(R)$. The above case corresponds to $\mathcal{F}(R) = R$.

In order to progress with analytical techniques we make a special choice for a localized $R_0(x)$ which allows for a closed expression for the integral of the coordinate map in equation (7a). Below, we will demonstrate by an explicit numerical integration of the coordinate map for a generic Gaussian perturbation $R_0(x)$ that the following results are robust with respect to the precise form of the perturbation. Thus we proceed with the choice

$$R_0(x) = W\left[r_0 e^{r_0-|x|/\delta}\right]. \tag{9}$$

for the initial profile. This profile decays exponentially at large $|x|$ and has a amplitude of r_0. For the relevant limit of $r_0 \ll 1$ the width at half amplitude is $\delta \ln 2$. This form is adapted to the integral in equation (7a) since the latter equation can be written as

$$t(\alpha,\beta) = -\alpha - \beta + \int_{-\alpha}^{\beta} \frac{\partial_{\beta'} R(\alpha,\beta')d\beta'}{\partial_{\beta'}(\ln R_0(-\beta')) - R_0'(-\beta') - Z_0'(-\beta')} \tag{10}$$

and $R_0(x)$ of equation (9) has the property that

$$\partial_x(\ln R_0(-x)) - R_0'(-x) = -\frac{1}{\delta}\mathrm{sgn}(x). \tag{11}$$

For the static phase we will consider always a profile with a constant slope,

$$Z_0(x) = mx, \tag{12}$$

where due to our definition of Z the parameter m measures the *excess* slope relative to the critical angle. For these initial data the solution of equations (4) in the curved coordinate frame reads

$$R(\alpha,\beta) \;=\; W\left[r_0 e^{r_0-|\beta|/\delta-m(\alpha+\beta)}\right] \tag{13a}$$

$$Z(\alpha,\beta) \;=\; m\alpha. \tag{13b}$$

In order to integrate the equations for the coordinate mapping, see equation (7a), we have to divide the space-time into different sectors due to the sign function of equation (11). Depending on the sign of α and β we define the following three sectors, (I): $\alpha \le 0$, $\beta > 0$, (II): $\alpha \le 0$, $\beta \le 0$, and (III): $\alpha > 0$, $\beta \le 0$. The case α, $\beta > 0$ is mapped to negative times, and is therefore not of interest. The boundary between the sectors (II) and (III) in the $t-x$ plane can be obtained by integrating equation (7a) with $\alpha = 0$ and $\beta < 0$. The boundaries are given by

$$x_{\mathrm{I/II}}(t) \;=\; -t, \tag{14a}$$

$$x_{\mathrm{II/III}}(t) \;=\; \frac{r_0}{m-1/\delta}\left(e^{(m-1/\delta)t}-1\right), \tag{14b}$$

where the subscript indicates the adjacent sectors, see figure 4.

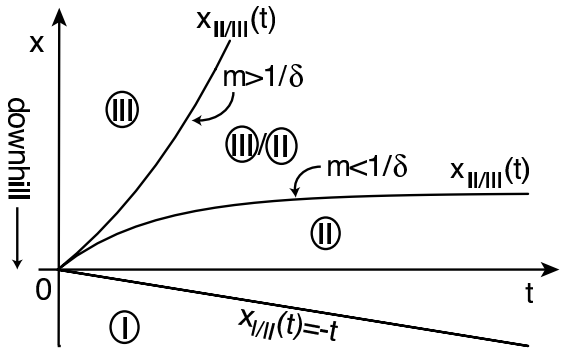

FIG. 4: Model $\mathcal{P}$: Boundaries between different sectors in the $t-x$ plane.

In sectors (I) and (III) an explicit expression for the profiles can be obtained. From the integrated version of equation (7a) one easily gets the result

$$R(t,x) = R_0(\alpha(t,x))e^{(m\pm 1/\delta)t}, \tag{15}$$

where $\pm$ refers to sector (I), (III), respectively. Together with equation (13b) this result shows that the system has a simple time evolution along the characteristic curves of constant $\alpha(t,x)$. Using equations (13b), (15) and $\beta = -t-x$, we obtain the explicit expression for the coordinate mapping in sector (I),

$$\frac{1}{m}Z(t,x) = \alpha(t,x) = x + \frac{1-e^{(m+1/\delta)t}}{m+(1/\delta)e^{(m+1/\delta)t}} W\left[\frac{r_0}{m+1/\delta}e^{r_0+x/\delta}\left(m+(1/\delta)e^{(m+1/\delta)t}\right)\right]. \tag{16}$$

The result for sector (III) is obtained from the latter expression by the replacement $\delta \to -\delta$. equations (15), (16) are our final result for the profiles in sectors (I) and (III). In sector (II) the characteristic curves $x_\alpha(t)$ which maps to a constant α can be obtained again explicitly but we were unable to invert them to obtain $\alpha(t,x)$. The characteristic curves read

$$x_\alpha(t) = \frac{1}{m-1/\delta}\left[h(\alpha)e^{(m-1/\delta)t} + \ln(h(\alpha)/r_0) + m\alpha - r_0\right] \tag{17}$$

with the function

$$h(\alpha) = W^{\frac{2/\delta}{m+1/\delta}}\left[r_0 e^{r_0-m\alpha}\right] W^{\frac{m-1/\delta}{m+1/\delta}}\left[r_0 e^{r_0+\alpha/\delta}\right]. \tag{18}$$

As in sectors (I) and (III) the curves behave exponentially in time with, however, more complicated amplitudes. The characteristic curves are shown for $r_0 = 0.1$, $\delta = 5.0$ and different slopes m in figure 5.

With the characteristic curves at hand, the solutions for $R(t,x)$ and $Z(t,x)$, at a fixed time, are given in parametric form in the $x-R$ or $x-Z$ plane by the curves $[x_\alpha(t), R(\alpha,\beta=-x-t)]$, $[x_\alpha(t), m\alpha]$, respectively, with α as running parameter.

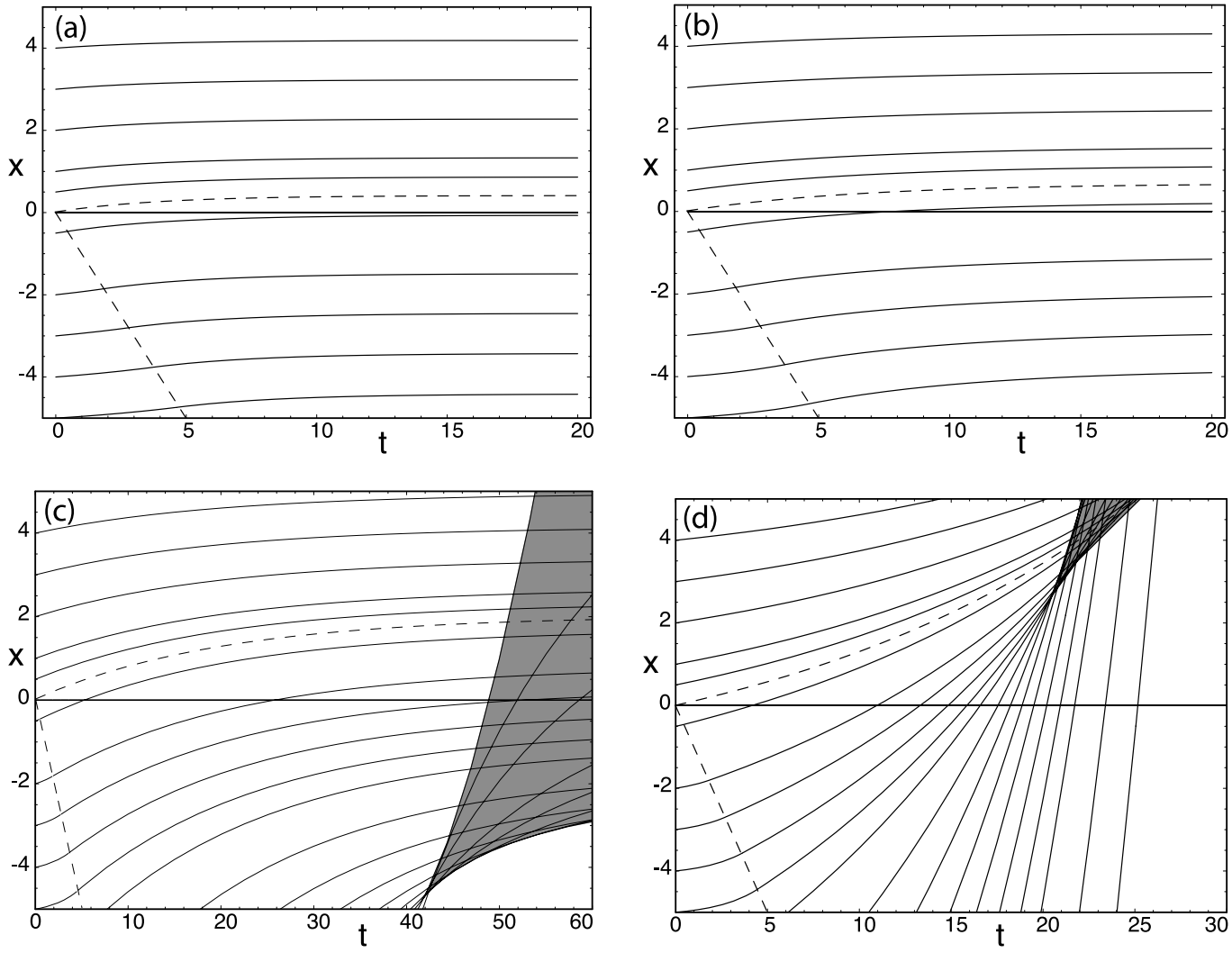

FIG. 5: Model $\mathcal{P}$: Characteristic curves with constant α for a perturbation $R_0(x)$ of Eq. (9) with $r_0 = 0.1$, $\delta = 5.0$ and slopes (a) $m = -0.05$, (b) $m = 0.05 < 1/\delta$, (c) $m = 0.15 < 1/\delta$ and (d) $m = 0.25 > 1/\delta$. The shaded area indicates the region with shocks. The dashed curves mark the boundaries between the different sectors, cf figure 4.

2. Appearance of shocks

Before we discuss the resulting profiles, we will study the possibility for the occurrence of shocks, i.e., discontinuities of the profiles which develop at a finite time. Such kind of singularities are possible for non-linear dynamics since adjacent characteristic curves can bend differently, leading even for small differences in curvature at small times to intersecting curves at larger times. Beyond the time at which the curves cross for the first time, there is a region where a unique solution no longer exists. Two such situations are visualized for our model in figures 5(a) and (c). If characteristic curves cross each other they form an envelope. The shock position is then determined by the cusp of the envelope. While we leave the precise definition and the calculation of the envelope to Appendix B, we discus here the criterion for the existence of shocks in our model. We are interested in not too large amplitudes r_0. For $r_0 < \sqrt{2}$, there is a simple condition for the formation of shocks. Then it can be shown, see Appendix B, that shocks occur only if the slope of the profile of the resting grains is larger than the critical value

$$m_c = \frac{\sqrt{2}-1}{\delta}. \tag{19}$$

Thus for broad perturbations in the moving phase shocks occur already for small slopes m. The exact time t_s and position of the shock is in general difficult to calculate. For sufficiently large m ($m > 1/(2r_0\delta)$ if $r_0 < 1$ and $m > 1/(\delta(1+r_0))$ if $r_0 > 1$) an exact expression can be obtained and is given in Appendix B. On the other hand, for

slopes close the critical one the shock time diverges as

$$t_s \sim (m - m_c)^{-1}. \tag{20}$$

For our above choice of parameters r_0 and δ for figure 5 the critical slope is $m_c = 0.0828$.

3. *Different avalanche dynamics*

Figure 5 shows four possible situations: (a) A slope m which is larger than critical m_c but smaller than $1/\delta$ so that the characteristic curves saturate at large times, (b) a slope smaller than the critical m_c, (c) a slope which is larger than both the critical m_c and $1/\delta$ so that the curves grow exponentially in time, and (d) the case of a negative m. The solutions for the corresponding profiles of $R(t, x)$ and $Z(t, x)$ are shown in parts (a) of figures 6 - 8. Plotted are the two curves $Z(t, x) - mx$ (always corresponding to the lower curve) and $Z(t, x) - mx + R(t, x)$ so that the gap between the two curves represents the layer of moving grains. The maximum of the perturbation propagates downhill with a constant velocity which is 1 in our rescaled units. For a negative slope m (corresponding to an actual slope smaller than the angle of repose) all grains of the perturbation come finally to rest, generating a bump on the initial static profile which corresponds to the baseline in the plot, see figure 6(a). The amplitude of the perturbation decays exponentially at large times, $R(t, x = -t) \simeq r_0 \exp(r_0 + mt)$. If we define the downhill end of the bump by the condition that the maximum of the perturbation in $R(t, x)$ has decayed to some fraction $\epsilon \ll 1$ of the initial amplitude, then the width of the bump scales like $\ln(\epsilon)/m$ for small r_0 since the peak in $R(t, x)$ moves with a velocity of one. Thus the final width of the deposited amount of grains is independent of the amplitude and width of the perturbation but only determined by the initial slope of the static phase. For positive slopes m the amplitude $R_{\max}$ of the perturbation grows at large times linear,

$$R_{\max} \simeq m(1 + m\delta)\, t, \tag{21}$$

with a growth rate which is independent of the initial amplitude r_0. However, there is a broad transient behavior with logarithmic corrections at intermediate time scales. The exponential time behavior found at the beginning of this section for an initially homogeneous mobile phase is recovered for $m < 0$ but is in contrast to the linear growth for positive m.

For both positive and negative initial slopes, the profile $Z(t, x)$ of the static phase does no longer evolve after the avalanche has passed. The resulting profile $Z_\infty(x)$ becomes thus time independent for times larger than a (position dependent) time scale. This asymptotic profile is only well defined if no shock occurs. In the latter case it is implicitly given by

$$\frac{1}{m - 1/\delta} \left[\ln\left(\frac{h(Z_\infty(x)/m)}{r_0} \right) + Z_\infty(x) - r_0 \right] = x, \tag{22}$$

where the function h is given by equation (18). The latter expression is valid in sector (II) which is the relevant region for large times, see figure 4. From this result one can obtain the slope $\partial_x Z_\infty$ at a given value of Z,

$$\partial_x Z_\infty(x) = (m - 1/\delta) \left[\frac{h'(Z_\infty(x)/m)}{m h(Z_\infty(x)/m)} + 1 \right]^{-1}. \tag{23}$$

The behavior of Z_∞ depends on the sign of m. For negative m the deposited grains form a bump that was described above and whose exact shape is given by equation (22). Across this bump, we find that the change of the slope as compared to the initial slope m is always rather small. Far away from the bump (at large positive and negative x) one has $h'/h \simeq -1/\delta$, and thus $\partial_x Z_\infty = m$ remains, of course, unchanged from the initial profile. For positive m the profile $Z(t, x)$ shows again a constant slope after the avalanche has passed, i.e., $Z_\infty = m_\infty x$, cf figure 7. The asymptotic slope can be obtained from the behavior of the function h at large negative arguments. We find

$$m_\infty = m \left[1 + \left(\frac{2m}{m\delta + 1 + \sqrt{2}} \right) \left(\frac{1}{m_c - m} \right) \right]. \tag{24}$$

Interestingly, the relative change of the slope is independent of the amplitude r_0 of the perturbation and depends only on the product of the initial slope m and the width δ of the perturbation. Surprisingly, the expression in the square brackets in equation (23) is larger than one for positive m, and even diverges as the slope m approaches the critical value m_c beyond which shocks occur, $m_\infty \sim (m_c - m)^{-1}$. It is important to note that the layer of moving grains decays to zero at large times at the uphill end of the avalanche, although the slope of the static layer is steeper than

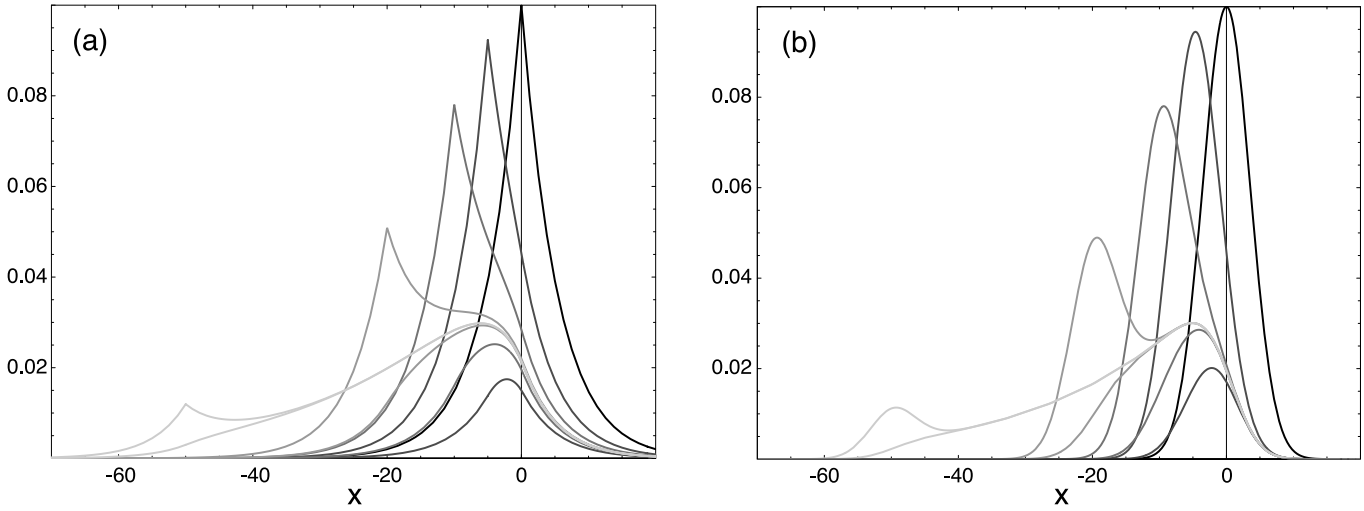

FIG. 6: Model $\mathcal{P}$ with $b = 0$: Fixed time profiles $Z(t,x) - mx$ and $R(t,x) + Z(t,x) - mx$ so that the gap between two corresponding curves represents the thickness of the mobile phase. Plot (a) is for $R_0(x)$ of Eq. (9) and (b) for a Gaussian $R_0(x)$, both for $m = -0.05$. The profiles are for times $t = 0$, 5, 10, 20 and 50. Here and in the following plots of profiles the plotting intensity decreases with increasing time.

before the avalanche started. This behavior can be easily understood from the property of equation (4) in which the exchange between the static and rolling phase is proportional to R. Of course, physically, there will be a maximum angle for the stability (even for $R = 0$) beyond which the above predictions are irrelevant, and an extended model has to be considered.

An important quantity is the total size of the avalanche. Within our model, we define the size $I(t)$ of an avalanche as the spatially integrated amount of mobile grains, i.e.,

$$I(t) = \int_{-\infty}^{\infty} R(t,x)\, dx\,. \tag{25}$$

The integration can be performed for each sector separately by a change of variables to the characteristic coordinate α. The contribution from sector (III) can be neglected at larger times since the avalanche starts at $x = 0$ to propagate to the left (downhill), cf figure 4. For negative m, the perturbation decays exponentially, and thus we obtain for the size

$$I(t) = 2r_0\delta\, e^{r_0+mt}. \tag{26}$$

For positive m we observe that the size of the avalanche shows a quadratic increase in time,

$$I(t) = m^2\delta\, \frac{1+m\delta}{1-m\delta}\, t^2, \tag{27}$$

at asymptotically large times. Interestingly, the growth of the avalanche depends only on its initial width δ but not on the amplitude r_0. By comparison with the scaling of the amplitude of the avalanche, cf equation (21), we observe that the width of the avalanche must grow also linear in time $\sim m\delta/(1-m\delta)t$.

So far we have studied mainly an initial perturbation which is particularly suited for obtaining analytical results. In order to check the robustness of our results with respect to the precise form of $R_0(x)$ we have chosen also a Gaussian $R_0(x) = r_0 \exp(-x^2/\delta^2)$ together with the same $Z_0(x) = mx$ as before. Contrarily to the previous case, the initial perturbation has no cusp at $x = 0$. By a numerical computation of the integral of equation (7a) we obtained the profiles shown in parts (b) of figures 6 - 8, using $r_0 = 0.1$, $\delta = 5$ as before. As can be observed from the plots the characteristic features can be regarded as robust. However, the moving layer, i.e., the gap between the upper and lower graph decays more rapidly due to the faster decay of the Gaussian profile. Of course, the critical slope m_c for shocks is no longer given by equation (19). We observe that for the Gaussian $R_0(x)$ shocks occur only beyond a m_c which is *increased* compared to the exponentially decaying profile of equation (9) with the same width at half height, cf figure 8.

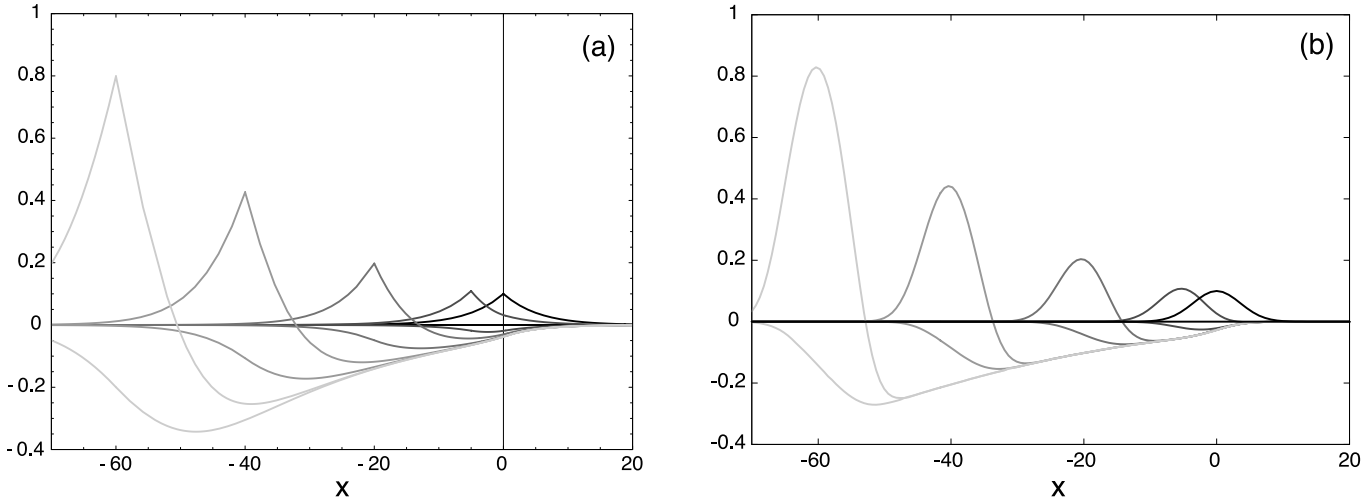

FIG. 7: Analog of Fig. 6 but for $m = 0.05$ and times $t = 0$, 5, 20, 40 and 60.

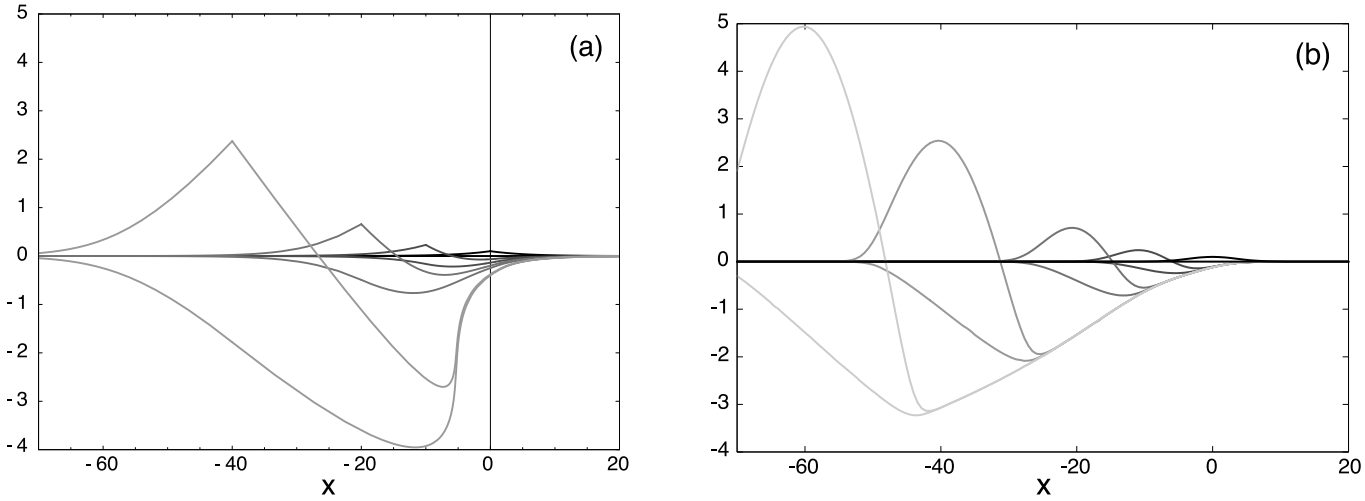

FIG. 8: Analog of Fig. 6 but for $m = 0.15$ and times $t = 0$, 10, 20, 40 and 60 for (b) only. In plot (a) a shock occurs at the uphill end of the avalanche (shock time $t_s = 41.71$). Note that for the Gaussian $R_0(x)$, plot (b), shocks are generated only for larger values of m, see text.

B. Strong stress anisotropy: small b

1. *Analytical result for general slopes m*

So far we have assumed such a strong stress anisotropy that there is no horizontal stress σ_{xx}, i.e., $b = 0$ in the model of equation (4). In this section we will study the influence of a small σ_{xx} on the avalanche dynamics we found in the previous section. Although steady state simulations suggest a value of b close to one [17, 18], it is interesting to study the regime of small b in order to compare to the BCRE model. The method of characteristics can be applied of course to arbitrary values of b, yielding a system of equations which we could not solve explicitly so that we had to resort to a perturbative treatment. Thus, we consider the terms proportional to b in equation (4) as small perturbations of the $b = 0$ solution. This can be done by the following ansatz

$$Z = Z_1 + bZ_2 \tag{28a}$$
$$R = R_1 + bR_2, \tag{28b}$$

where Z_1 and R_1 denote the solution for $b = 0$ of the previous section. Although one expects realistic values of b of order unity, the perturbative calculation should allow for a qualitative assessment of the effect of a finite horizontal

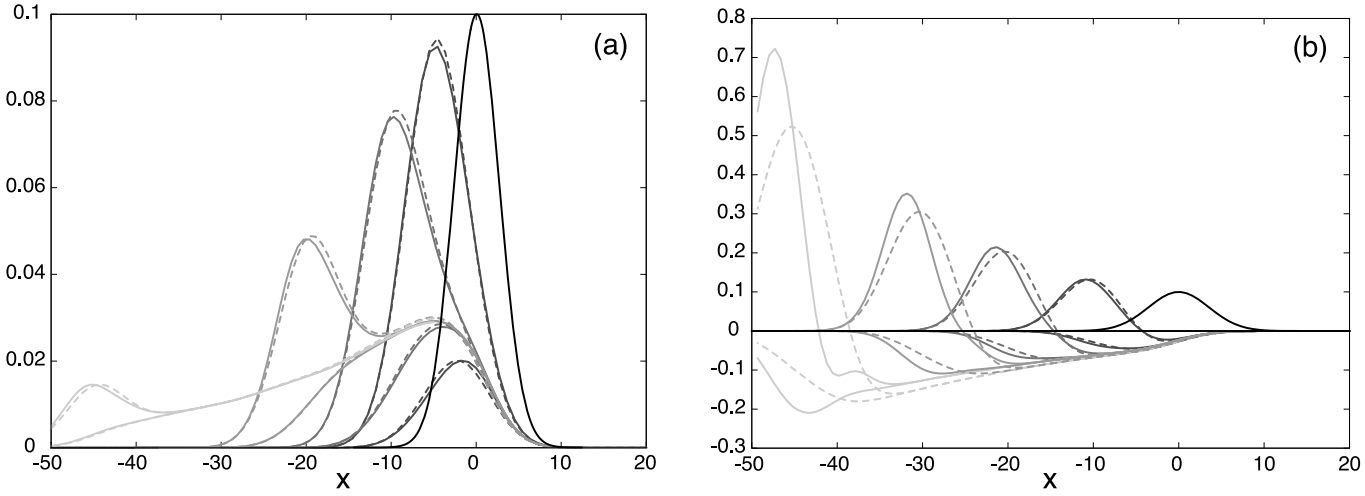

FIG. 9: Model $\mathcal{P}$ with finite $b = 0.5$: Profiles for a Gaussian $R_0(x)$ and (a) $m = -0.05$ (for $t = 0$, 5, 10, 20 and 45), (b) $m = 0.05$ (for $t = 0$, 10, 20, 30 and 45). The dashed curves represent the corresponding profiles for $b = 0$ of section III A and are shown for comparison.

stress. The dynamics of the corrections are then described by the following *linear* coupled equations

$$\partial_t Z_2 = -R_1 \left(\partial_x Z_2 + \partial_x R_1\right) - R_2 \partial_x Z_1 \tag{29a}$$

$$\partial_t R_2 = \partial_x R_2 + R_2 \partial_x Z_1 + R_1 \left(\partial_x Z_2 + \partial_x R_1\right) . \tag{29b}$$

Since we consider corrections of linear order in b, the terms containing derivatives of the profiles R_2 and Z_2 have exactly the same form as those in equation (4) with $b = 0$. Thus, the characteristic directions $\zeta_+ = -1$, $\zeta_- = R_1$ and characteristic curves remain unchanged for small b. In terms of the characteristic coordinates α and β, the corrections obey the equations

$$\partial_\alpha Z_2 + \frac{1+R_1}{R_1}\partial_\alpha R_2 - \left(\frac{R_2}{R_1}\partial_x Z_1 + \partial_x R_1\right)\partial_\alpha t = 0 \tag{30a}$$

$$\partial_\beta Z_2 + \left(R_2 \partial_x Z_1 + R_1 \partial_x R_1\right)\partial_\beta t = 0. \tag{30b}$$

Here all functions have to be considered as depending on α and β, in particular $t(\alpha, \beta)$ is given by equation (7a). In order to express the derivatives with respect to x as functions of α, β, we use $\partial_x = \partial_x\alpha\,\partial_\alpha + \partial_x\beta\,\partial_\beta$ together the relations

$$\partial_x\beta = -1, \quad \partial_x\alpha = \frac{1}{1+R_1}\frac{1}{\partial_\alpha x} \tag{31}$$

with $x(\alpha, \beta)$ given by equation (7b). Using these relations and the solutions for $b = 0$ of equation (8) with the initial condition $Z_0(\alpha) = m\alpha$, the equation (30) can be rewritten after integration over α as

$$Z_2 + \frac{1+R_1}{R_1} R_2 + \ln\left(\frac{1+R_1}{1+R_0(-\beta)}\right) - \int_{-\beta}^{\alpha} d\alpha' \partial_\beta R_1(\alpha', \beta)\partial_{\alpha'} x(\alpha', \beta) = 0 \tag{32a}$$

$$\partial_\beta Z_2 + \frac{R_1}{1+R_1}\partial_\beta R_1 + \frac{m}{(1+R_1)^2 \partial_\alpha x}\left(\frac{R_1^2}{1+R_1} - R_2\right) = 0, \tag{32b}$$

where the functions depend on α and β unless arguments are written explicitly. The explicit expression for $\partial_\alpha x$ can be obtained from the solution for $b = 0$, leading to

$$\partial_\alpha x = \frac{1}{1+R_0(\alpha)} - \int_{-\alpha}^{\beta} d\beta' \frac{\partial_\alpha R_1(\alpha, \beta')}{[1+R_1(\alpha, \beta')]^2}. \tag{33}$$

The function R_2 can be eliminated from equation (32b) by using equation (32a), and the resulting linear ordinary differential equation for Z_2 can be integrated easily. The result is

$$Z_2(\alpha, \beta) = \exp\left[\int_{-\alpha}^{\beta} d\beta' g_1(\alpha, \beta')\right] \int_{-\alpha}^{\beta} d\beta' g_2(\alpha, \beta') \exp\left[-\int_{-\alpha}^{\beta'} d\beta'' g_1(\alpha, \beta'')\right], \tag{34}$$

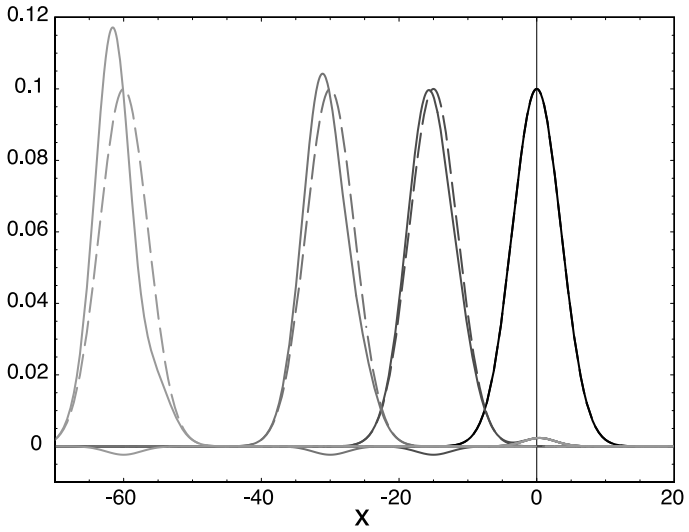

FIG. 10: Model $\mathcal{P}$ at the angle of repose ($m = 0$) for finite horizontal stress, $b = 0.5$: Profiles for a Gaussian $R_0(x)$ at times $t = 0$, 15, 30 and 60. The dashed curves correspond to the absence of horizontal stress, $b = 0$, where the perturbation R_0 propagates without changing its shape.

with the functions

$$g_1(\alpha,\beta) = -\frac{mR_1}{(1+R_1)^3\partial_\alpha x} \tag{35a}$$

$$g_2(\alpha,\beta) = -\frac{R_1}{1+R_1}\partial_\beta R_1 - \frac{mR_1}{(1+R_1)^3\partial_\alpha x}\left\{R_1 + \ln\left(\frac{1+R_1}{1+R_0(-\beta)}\right) - \int_{-\beta}^{\alpha} d\alpha' \partial_\beta R_1(\alpha',\beta)\partial_{\alpha'} x(\alpha',\beta)\right\}. \tag{35b}$$

This is our final result for Z_2, the profile R_2 can be computed now from equation (32a). Using the explicit result for R_1 of equation (8b) the multiple integrals can be performed easily numerically. The resulting profiles are shown in figures 9 for the parameters r_0, δ and m of section III A with $b = 0.5$. For comparison the solution for $b = 0$ are also shown as dashed curves. As can be seen from figure 9(a), for negative m the avalanche and the static profile are not much effected by the presence of horizontal stress $\sim b$. In contrast, for positive slopes m there is more visible effect of the horizontal stress. This effect grows with increasing time scale, cf figure 9(b). As one could naively expect, horizontal stress has the tendency to shift the peak in dynamics phase downhill (to the left). This shift will be analyzed quantitatively below for the case $m = 0$ and by comparing the numerical results of figures 9- 10 the shift appears to be independent of m. For the static profile $Z(t,x)$ the horizontal stress leaves the final slope after the avalanche almost unchanged but it produces a steeper slope in $Z(t,x)$ where the moving layer $R(t,x)$ has maximal thickness. There is also a tendency for the static profile to form a local dell at the peak of the avalanche, see figure 9(b). This observation becomes especially pronounced for $m = 0$, see figure 10.

2. Explicit results at the angle of repose ($m = 0$)

It is obvious form the structure of equations (34)-(35b) that major simplifications occur if the initial static profile is exactly at the angle of repose, i.e., $m = 0$. Thus, we can study easily the effect of a horizontal stress (finite b) in this situation. Let us first summarize the results in the absence of horizontal stress ($b = 0$) when $m = 0$. The static layer stays for all times at the angle of repose, $Z_1(t,x) = 0$, and the initial perturbation $R_0(x)$ in the moving layer simply propagates downhill, $R_1(t,x) = R_0(t+x)$. Thus the amount of grains in both the static and the moving layer are conserved. The situation is different for finite b. The layers of static and dynamic grains, respectively, have coupled dynamics with the corrections from finite b given by

$$Z_2(\alpha,\beta) = R_0(\alpha) - R_0(-\beta) + \ln\left(\frac{1+R_0(-\beta)}{1+R_0(\alpha)}\right) \tag{36a}$$

$$R_2(\alpha,\beta) = \frac{R_0(-\beta)}{1+R_0(-\beta)}\left\{R_0'(-\beta)t(\alpha,\beta) - Z_2(\alpha,\beta)\right\}, \tag{36b}$$

where the mapping between t, x and α, β has for $m = 0$ the simple form

$$t(\alpha,\beta) = -\int_{-\alpha}^{\beta} \frac{d\beta'}{1+R_0(-\beta')} \tag{37a}$$

$$x(\alpha,\beta) = -t(\alpha,\beta) - \beta\,. \tag{37b}$$

These equations provide a closed parametric form of the dynamics for a general initial perturbation $R_0(x)$. The resulting time evolution of a Gaussian perturbation $R_0(x) = r_0 \exp(-x^2/\delta^2)$ is shown in figure 10. Compared to the absence of horizontal stress, $b = 0$, there are a number of interesting novel features. The avalanche amplitude increases and the maximum is shifted downhill. The layer of static grains displays a bump at the initial position of the perturbation and a dell which propagates downhill close to the maximum of the avalanche peak. At large times, equation (37a) leads to $\alpha \simeq x$ which together with $\beta = -x - t$ and equation (36) yields an explicit expression for the profiles. For a small avalanche amplitude r_0, the position of the peak follows $x = -t - \delta/2$ for a Gaussian $R_0(x)$. The maximum of $R(t,x)$ grows linearly with time, $R_{\max} \sim b(r_0^2/\delta)t$, while in the absence of horizontal stress ($b = 0$) it remains constant. Notice that this linear growth was observed for $b = 0$ only at angles larger than the repose angle ($m > 0$), cf equation (21). The form of the static profile $Z(t,x)$ can be directly obtained from equation (36a). There are two identical contributions which are shifted relative to each other by t. The first contribution is approximately given by $b[R_0(x) - \ln(1 + R_0(x))]$. This term represents the bump at the start position of the avalanche. The second contribution has x replaced by $x + t$, corresponding to the dell traveling with the avalanche downhill, cf figure 10. Thus, both structures in the static layer are determined by the initial profile of the perturbation in the moving layer.

IV. LINEAR VELOCITY PROFILE (MODEL $\mathcal{L}$)

It has been argued that a constant velocity profile, as assumed in the previous Section, is only applicable to thin surface flow [26]. For a thicker layer of rolling grains, the velocity should depend on the amount of mobile grains. Experiments and simulations for steady deep systems suggest a linear profile for the average horizontal velocity $u(x,y) = \gamma y$ of the flow. With this profile we have $U = \frac{1}{2}\gamma R$, $W = \frac{1}{3}\gamma^2 R^2 = \frac{4}{3}U^2$ and the conservation conditions of equations (1) and (2) yield the model

$$\partial_t Z = -\partial_x Z - b\,\partial_x R, \tag{38a}$$

$$\partial_t R = R\,\partial_x R + \partial_x Z + b\,\partial_x R. \tag{38b}$$

Here all lengths are divided by g/γ^2, and time is divided by γ. Again, Z is replaced by $Z + \mu x$. The model contains after this rescaling only one free parameter, b. It is rather important to note that the latter model is valid only as long as R remains positive since we obtained it from equation (2) after division by R. Thus the actual solution of equation (38) is given by the maximum of $R = 0$ and the formal solution for R of equations (38a) and (38b). In this Section we will study the consequences of a R dependent linear velocity profile both in the absence ($b = 0$) and presence ($b \neq 0$) of horizontal stress. We note that for an initially uniform amount of rolling grains $R_0(x) = \varrho$ and a static sand bed with constant slope $Z_0(x) = mx$ the solution to Eqs. (38) is rather simple. As opposed to the exponential growth for model $\mathcal{P}$, the thickness of the mobile layer increases here only linear in time, $R(t,x) = \varrho + mt$ and $Z(t,x) = m(x-t)$ decreases accordingly. As for model $\mathcal{P}$ this solution is independent of b.

A. Infinite stress anisotropy ($b = 0$)

1. *Analytical solution*

In the limit of $b = 0$ the equations (38a) and (38b) are decoupled. Such set of equations has been studied by de Gennes et al. to describe a thick flow of granular matter in a bounded geometry [26]. Here we consider this simple model in an *unrestricted* geometry but we allow for general initial profiles $R_0(x)$ and $Z_0(x)$. Following again the approach outlined in Appendix A, we obtain the characteristic equations

$$\partial_\alpha x - \zeta_+ \partial_\alpha t = 0, \tag{39a}$$

$$\partial_\beta x - \zeta_- \partial_\beta t = 0, \tag{39b}$$

$$-\partial_\alpha Z + (\zeta_+ - 1)\,\partial_\alpha R = 0, \tag{39c}$$

$$-\partial_\beta Z + (\zeta_- - 1)\,\partial_\beta R = 0, \tag{39d}$$

with the characteristic directions given in the case of $b = 0$ by

$$\zeta_+ = 1, \quad \zeta_- = -R. \tag{40}$$

Since one of the characteristic directions is constant, these equations can be integrated in a way which is similar to the procedure we used for model with a constant velocity profile in section III A. From this calculation one finds easily that the general solution of equations (38) with $b = 0$ reads

$$\begin{aligned} t(\alpha,\beta) &= \int_{-\alpha}^{\beta} \frac{d\beta'}{1+R(\alpha,\beta')}, && \text{(41a)}\\ x(\alpha,\beta) &= -\beta + t(\alpha,\beta), && \text{(41b)}\\ R(\alpha,\beta) &= -1 + \sqrt{[R_0(\alpha)+1]^2 + 2[Z_0(\beta) - Z_0(-\alpha)]}, && \text{(41c)}\\ Z(\alpha,\beta) &= Z_0(-\beta). && \text{(41d)} \end{aligned}$$

Studying the configurations we studied in section III A for model $\mathcal{P}$ with a constant velocity profile, we choose $Z_0(x) = mx$ so that the integral in equation (41a) can be computed explicitly. One obtains, using (41c):

$$\begin{aligned} t(\alpha,\beta) &= \frac{1}{m}\left[\sqrt{[R_0(\alpha)+1]^2 + 2m(\alpha+\beta)} - R_0(\alpha) - 1\right] \\ &= \frac{1}{m}\left[R(\alpha,\beta) - R_0(\alpha)\right]. \end{aligned} \tag{42}$$

Since in the limit $b = 0$ equation (38a) acquires a simple linear form, we have obviously the result

$$Z(t,x) = Z_0(x-t) = m(x-t)\,. \tag{43}$$

At sufficiently large times one has $\alpha \sim x + mt^2/2$, and thus equation (42) shows that the amount of rolling grains is given by

$$R(t,x) = R_0(\tilde{x}) + mt \quad \text{with} \quad \tilde{x} \equiv x + \frac{m}{2}t^2\,. \tag{44}$$

2. Physical discussion

From the above result, the shape of the perturbation at a given large time would be the same for all initial slopes m. From this result, the maximum of the mobile layer $R(t,x)$ travels with a velocity $v_{\max} = r_0 + mt/2$ which, for $m > 0$, increases linear in time, i.e., the perturbation feels a *constant acceleration*. This has to be compared to the *constant velocity* we found for the model with a constant velocity profile, see section III A. However, for negative m, as explained above, the actual solution is obtained by setting $R(t,x)$ to zero in regions where it would be negative otherwise. At the time at which $R(t,x)$ becomes zero, the profile $Z(t,x)$ is frozen at its present height. Due to this construction the final solution for $Z(t,x)$ will deviate from the simple form of equation (43). For positive m the profile $R(t,x)$ as obtained from equation (42) is always non-negative. But there is the possibility that shocks actually prevent the system to reach the asymptotic time result of equation (44). In fact, independent of the initial parameters of R_0 and m, a shock *always* occurs after a finite time t_s, unless the solution $R(t,x)$ of equation (44) becomes formally negative (for negative m) before the shock can appear. The shock time is given by the general expression

$$t_s = \frac{1}{\max R_0'(x)}. \tag{45}$$

Remember that for the plug flow $\mathcal{P}$ model (see section III), a shock appears only for slopes m which are larger than a positive critical slope. For the model discussed here, shocks can even occur at negative slopes m.

In the following, we will consider again a Gaussian perturbation in the layer of rolling grains, $R_0(x) = r_0 \exp(-x^2/\delta^2)$. Then the shock time is $t_s = \sqrt{e/2}\,\delta/r_0$. Figure 11 shows the time evolution of this perturbation for both positive and negative m. Plotted are the profiles $Z(t,x) - mx$ and $Z(t,x) - mx + R(t,x)$ so that again the gap between the profiles corresponds to the layer of rolling grains. For negative m all moving grains have come to rest at the time $t = -r_0/m$ which is smaller than the shock time scale t_s for the parameters used here. For positive m there is an uniform increase in the thickness of the layer of rolling grains, see figure 11(b). This increase is linear in time, $\sim mt$, and is unrelated to the amplitude of the local perturbation $R_0(x)$. This apparently unphysical result

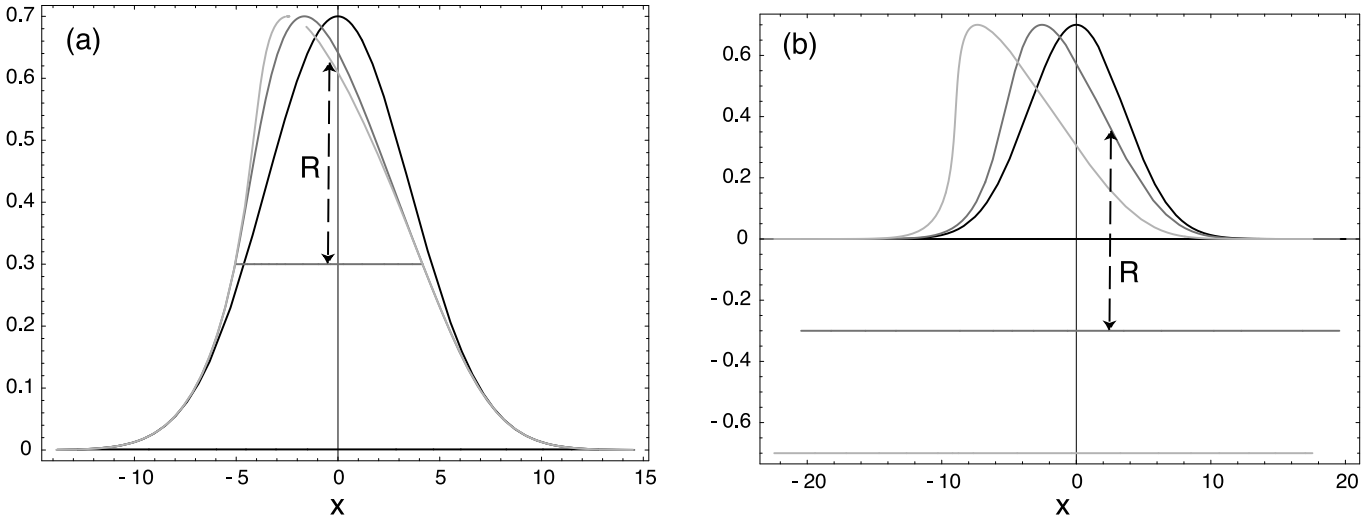

FIG. 11: Model $\mathcal{L}$ with $b = 0$: Profiles for a Gaussian profile $R_0(x)$ with $r_0 = 0.7$, $\delta = 5.0$ and slope (a) $m = -0.1$ (b) $m = 0.1$, both for times $t = 0$, 3 and 7. The shock time is $t_s = \sqrt{e/2}\delta/r_0 = 8.32$. For negative m the perturbation has stopped at the time $t = -r_0/m = 7.0$, i.e., the profile shown for the latter time is the final static profile. Note that for positive m the thickness of the moving layer shows an overall linear increase proportional to mt since for a Gaussian profile, $R_0(x)$ is in fact small but *finite* everywhere. For clarity, we indicated explicitly the thickness R of the mobile layer at $t = 3$.

can be understood from the structure of equation (38b). Even for a strictly localized initial $R_0(x)$ which is zero outside a finite interval, there would be an increase $\sim (\partial_x Z)t$ (for a constant slope) at all positions x, not only there where $R_0(x)$ is non-zero. But since we divided the original equations by R to obtain equation (38), $R = 0$ is a trivial solution. The latter solution should be matched with the finite R solution at the front of the avalanche. However, by definition, at the front the rolling layer becomes very thin, and a strictly linear velocity profile is certainly an oversimplification. Thus, with the model of this Section, the matching of the two solutions at the front is not justified. Instead, the dynamical equations should be refined as to describe the physical processes close to an avalanche front and the thin-to-thick flow crossover (for example along the lines of [26, 29]). This we leave to a future work.

B. Strong stress anisotropy: small b

1. *Analytical results*

Now we study the influence of finite horizontal stress with a finite but small b. An important consequence of a finite b is that now the equations (38) become coupled by the stress term. In order to obtain the dynamic response to a local perturbation we perturb about the $b = 0$ solution of the previous section. Following the analysis of section III B, we make the ansatz

$$Z = Z_1 + bZ_2 \tag{46a}$$
$$R = R_1 + bR_2, \tag{46b}$$

where Z_1 and R_1 denote the solution for $b = 0$ of the previous section, cf equations (41c) and (41d). By expansion of the equations (38) in b we obtain the dynamics of the contributions from finite b,

$$\partial_t Z_2 = -\partial_x Z_2 - \partial_x R_1 \tag{47a}$$
$$\partial_t R_2 = (1 + R_2)\partial_x R_1 + R_1 \partial_x R_2 + \partial_x Z_2. \tag{47b}$$

To this coupled system of equations we can again apply the method of characteristic curves. The resulting characteristic equations for the corrections to the profiles are

$$\partial_\alpha Z_2 + \partial_x R_1 \, \partial_\alpha t = 0, \tag{48a}$$
$$\partial_\beta Z_2 + (1 + R_1) \, \partial_\beta R_2 - [(1 + R_1)R_2 + R_1] \, \partial_x R_1 \, \partial_\beta t = 0, \tag{48b}$$

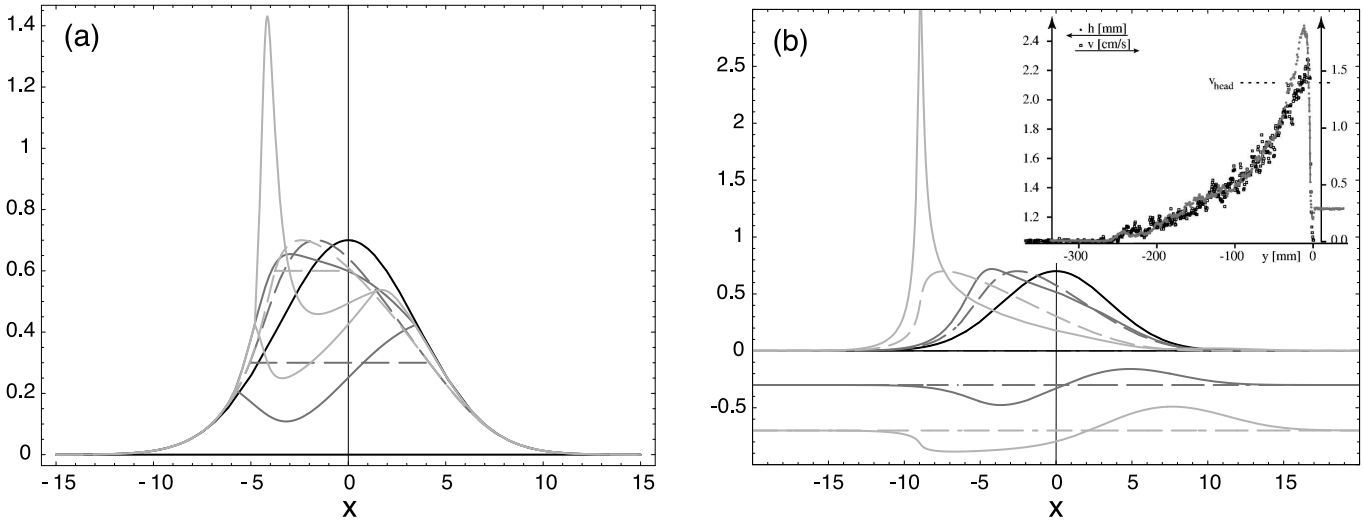

FIG. 12: Model $\mathcal{L}$ with finite $b = 0.5$ for the same parameters as in figure 11. The plots are for times (a) $t = 0$, 3 and 6, and (b) $t = 0$, 3 and 7. For comparison, the corresponding profiles for $b = 0$ are shown as dashed curves. Notice that the peak appears rather sharp due to the relative elongation of the vertical axis. Inset: For qualitative comparison, experimental results as given by Fig. 23 of Ref. 11 for the surface velocity v and the local height h of the mobile layer which corresponds to R in our notation. A linear relation between v and R is observed, and the shape of R resembles that of our analytical result. (The direction of flow is inverted in the experiment compared to our model.)

where the characteristic direction are the same as in the unperturbed case, $\zeta_+ = 1$, $\zeta_- = -R_1$. Again all functions in the above equations have to be regarded as depending on α, β. Derivatives with respect to x can be rewritten by the use of the relations

$$\partial_x \beta = -\left(\frac{R_1}{1+R_1}\right)^2, \quad \partial_x \alpha = \frac{\partial_\alpha R_1 - R_0'(\alpha)}{m(1+R_1)}. \tag{49}$$

Using the latter relations, equation (48a) can be integrated with respect to α. The result is

$$Z_2(\alpha,\beta) = -\int_{-\beta}^{\alpha} d\alpha' \frac{R_0'(\alpha')}{1+R_1(\alpha',\beta)}. \tag{50}$$

By inserting this solution into equation (48b) one obtains an ordinary differential equation (with respect to β) for $R_2(\alpha,\beta)$. In formal analogy to equation (34) its solution can be written as

$$R_2(\alpha,\beta) = \exp\left[\int_{-\alpha}^{\beta} d\beta' g_1(\alpha,\beta')\right] \int_{-\alpha}^{\beta} d\beta' g_2(\alpha,\beta') \exp\left[-\int_{-\alpha}^{\beta'} d\beta'' g_1(\alpha,\beta'')\right], \tag{51}$$

where the functions g_1 and g_2 are now given by

$$g_1(\alpha,\beta) = \frac{m}{(1+R_1)\left[R_0(\alpha) + m/R_0'(\alpha) - R_1\right]} \tag{52a}$$

$$g_2(\alpha,\beta) = \frac{1}{1+R_1}\left[R_1 g(\alpha,\beta) - \partial_\beta \ln(1+R_0(-\beta)) + m\int_{\alpha}^{-\beta} d\alpha' \frac{R_0'(\alpha')}{(1+R_1(\alpha',\beta))^3}\right]. \tag{52b}$$

Most of the integrals in equation (51) can be obtained in closed form. After a tedious calculation the final result can be expressed in terms of single integrals, that we give for completeness:

$$\begin{aligned} R_2(\alpha,\beta) &= \frac{1}{1+(R_0(\alpha)-R_1)R_0'(\alpha)/m}\left\{\frac{R_0'(\alpha)}{m}\left[R_1 - R_0(\alpha) - \ln\left(\frac{(1+R_1)(1+R_0(-\beta))}{(1+R_0(\alpha))^2}\right)\right]\right. \\ &+ \int_{-\alpha}^{\beta} d\beta' \frac{R_0'(-\beta')(1+(R_0(\alpha)-R_1(\alpha,\beta'))R_0'(\alpha)/m}{(1+R_1(\alpha,\beta'))(1+R_0(-\beta'))} - \frac{R_0'(\alpha)}{m}\int_{-\beta}^{\alpha} d\alpha' \frac{R_0'(\alpha')}{1+R_1(\alpha',\beta)} \\ &- \left.[1+(R_0(\alpha)+1)R_0'(\alpha)/m]\int_{-\beta}^{\alpha} \frac{R_0'(\alpha')d\alpha'}{(R_1(\alpha,\beta)+1)^2-(R_1(\alpha',\beta)+1)^2}\left[\frac{1+R_1(\alpha,\beta)}{1+R_1(\alpha',\beta)} - \frac{1+R_1(\alpha,-\alpha')}{1+R_0(\alpha')}\right]\right\} \end{aligned} \tag{53}$$

The equations (50) and (53) provide the final result for the changes in the profiles due to a finite horizontal stress. The solution is valid for *general* initial profiles $R_0(x)$. In figure 12 we have plotted this solution for a Gaussian perturbation with the same parameters as in the previous section, cf figure 11.

2. Physical discussion

The main difference coming from finite b is the generation of a peak at the downhill front of the avalanche, both for positive and negative slopes m. From the model of Eqs. (38) one observes that the term proportional to b is controlled by the slope of the moving layer. Since this slope becomes steeper at the downhill front with evolving time, there is an increasing thickness of the mobile layer close to the front. From a physical point of view this amplification can be understood from the effect of the horizontal stress which increases with R. Thus at the downhill front there is a net force which pushes the material towards the front and induces an extra growth of the rolling layer. As demonstrated by the inset of Fig. 11 our result is in qualitative agreement with measurements of the thickness of the mobile layer of grains along the symmetry axis of a triangular shaped avalanche moving on a static layer of limited thickness [11]. For positive m there is, in addition to the homogeneous and linear decrease of Z, a net transport of grains of the sand bed from the downhill front to the uphill end.

V. CONCLUSION AND DISCUSSION

In this paper, we have studied two sets of St Venant equations for the modeling of granular avalanches on an erodible bed. The models differ in the choice of the velocity profile within the flowing layer – either a plug flow ($\mathcal{P}$) or a profile with a constant velocity gradient ($\mathcal{L}$) – which give rise to different non-linearities. These models can been solved analytically by the method of characteristics, at least for sufficiently large stress anisotropy, and we have focused our attention on the situation where a uniform static slope is initially disturbed by a localized amount of rolling grains. We were able to compute the space and time evolution of the avalanche which either dies or grows, depending on whether the initial slope is below or above the angle of repose.

Such unsteady and non-uniform flows are very demanding for the models as the description of fronts and the generation of shocks must be addressed. For the case of a plug flow we found that shocks occur at the uphill end of the avalanche above a positive critical value m_c of the slope. Below this value, the asymptotic large time behavior can be computed, and we found that the amplitude and width of the avalanche grow linearly in time if $m > 0$, whereas for negative m the initial perturbation decays exponentially and the width of the deposited bump of grains scales like $1/m$. For a linear velocity profile, shocks occur for all slopes at a finite time that can be computed explicitly and is related to the shape of the initial distribution of rolling grains. By contrast to the previous case, shocks are located at the front of the avalanche.

Our analysis shows that these models predict several interesting qualitative features of granular avalanches, that can be compared with experiments. However, in the present form they also certainly have a number of shortcoming. The plug flow assumption, for example, is not tenable for a rolling layer thickness which starts to be of the order of several grain diameters, as particles on the top of such a layer would not feel the damping due to the friction on the static bed. On the other hand, the linear velocity hypothesis yields a vanishing velocity $U \to 0$ when the thickness of the mobile layer $R \to 0$, which forbids any front to move. However, shock-less and well defined propagative fronts are observed experimentally in steady [6] or unsteady [30] situations. Our model also does not correctly account for slope hysteresis which should differentiate between a starting and a stopping angle, $\phi_{\rm start}$ and $\phi_{\rm stop}$, respectively. In fact, the region between $\phi_{\rm stop}$ and $\phi_{\rm start}$ is precisely that of major interest as static slopes with an angle $\phi > \phi_{\rm stop}$ are stable but can generate growing avalanches when disturbed by a local amount of rolling grains. Because the non-linear terms in model $\mathcal{P}$ are all proportional to R, spontaneous avalanches (for $R = 0$) can never occur whatever the value of the initial slope. This would correspond to the maximal value of $\pi/2$ for $\phi_{\rm start}$. This, however, implies that model $\mathcal{P}$ can be applied to the experimentally important regime of slopes which are only slightly larger than $\phi_{\rm stop}$ and sufficiently small compared to $\phi_{\rm start}$. On the other hand, the uniformly growing solution for R in model $\mathcal{L}$ can be interpreted as evidence that both angles $\phi_{\rm start}$ and $\phi_{\rm stop}$ are identical so that beyond that angle avalanches occur even at $R = 0$ (unstable slope).

To include the above mentioned effects in the presented models, new directions have to be proposed. First, one can modify the dynamical equations itself while keeping their general structure (hyperbolic first order differential equations) with its analytic properties being tractable by the method of characteristics. Second, additional physical input could be used to either study the propagation of shocks beyond the shock time scale or one could implement boundary conditions on, e.g., the slope of the profiles to describe the dynamics close to the avalanche front. To be more specific, we discuss two points of particular interest: The velocity profile and hysteresis effects.

As proposed theoretically and demonstrated by experiments, an R-dependence of the flow velocity must be kept to allow for thick avalanches. The commonly used strictly linear velocity profile with the rheological ansatz $u(x, y) = \gamma y$ (constant shear rate) leads to problems at the avalanche front since the depth averaged velocity U should stay finite and of the order of $\sqrt{gd}$ when $R \to 0$. A possibility is to let γ diverge in this limit. This would correspond to a crossover from model $\mathcal{L}$ to model $\mathcal{P}$ below a certain small value for R of the order of a grain diameter d (see [26]). The corresponding matching of characteristic curves is technically involved and moreover such a treatment would not provide an understanding of the physical mechanism of velocity selection. In fact, close photos of the foot of the avalanche fronts reported in [6] show a small gas-like region where grains are ejected from the dense flow. This means that this zone is, in a sense, outside of the present modeling framework and thus could allow for a discontinuity in R, for example, or for imposing an extra constraint on the profiles R and Z or their derivatives – e.g. a fixed slope of the free surface as observed on propagative fronts. Another more fundamental approach would be to consider the velocity U as an independent dynamical field which a priori is not related to R by a fixed velocity profile. Such kind of description has been applied to granular flow on a *fixed* plane [7] so that Z is not a dynamical quantity.

Another feature of sand piles that should be included in the St Venant models discussed here is the hysteresis of avalanche dynamics as reflected by the existence of two critical angles. Experimentally it is observed that, at least for a fixed profile Z, the critical angles are actually functions of the thickness R of the mobile layer [7]. Since the friction coefficient μ is given by the tangent of the actual angle of the pile, a non-constant friction coefficient $\mu(R)$ is expected. Indeed, at the scale of a single grain, the starting angle depends on the depth of "traps" due to the roughness of the static bed [19]. Therefore one should expect an increased value of μ below a typical thickness $R_{\rm trap}$ (of the order of a grain diameter). This increased value determines then the staring angle $\phi_{\rm start}$ while the μ at large R corresponds to the stopping angle $\phi_{\rm stop}$. A sufficiently large value of the friction coefficient at small R would lead, for the points where $R \leq R_{\rm trap}$, to a "freezing" of the sand bed profile Z at its current value.

Both modifications, constraints on the profiles at the avalanche front and a friction function $\mu(R)$, do not change the general structure of the dynamical equations studied in the present paper. Thus, the method of characteristics and our predictions should prove useful for a better understanding and modeling of non-stationary granular flow.

Acknowledgments

We thank B. Andreotti for essential discussions and a careful reading of the manuscript. This work was supported by the PROCOPE program of EGIDE (P.C. and J.-P.B.) and DAAD (T.E.) and by the Deutsche Forschungsgemeinschaft through the Emmy Noether grant No. EM70/2-2 (T.E.). The LPMMH is UMR 7636 of the CNRS. P.C. was before associated with the Laboratoire des Milieux Désordonnés et Hétérogènes (UMR 7603).

APPENDIX A: METHOD OF CHARACTERISTIC CURVES

In this section a brief account of the general theory for systems of partial differential of first order and *hyperbolic* type is presented. Due to the relevance to granular flow problems we will concentrate on non-linear systems consisting of two equations for two functions of two independent variables. In the present context of this paper, the functions are R and Z and the independent variables correspond to space x and time t. For such systems a complete mathematical theory is available [31]. Our presentation will follow closely the latter reference.

For hyperbolic systems the notion of characteristic curves is the central concept. Before introducing the general theory, we would like to motivate the introduction of characteristic curves or coordinates. This concept is particularly adapted to the case where the number of equations equals the number of independent variables. In the present case of two equations, the objective of the method of characteristics is to introduce instead of (t, x) a new coordinate frame (α, β) so that along the two families of curves of constant coordinates α and β the partial differential equations reduce to *ordinary* differential equations with respect to α and β.

Let us demonstrate the method explicitly for the simple case of one linear partial differential equation for a function $f(t, x)$ of the form

$$a(t, x)\, \partial_x f + b(t, x)\, \partial_t f + c(t, x)\, f = 0. \tag{A1}$$

The initial value will be prescribed at zero time, $f(t = 0, x) = f_0(x)$. First, we have to define the characteristic curves $[t(\alpha), x(\alpha)]$ where α is a variable parameterizing a given curve. These curves are specified in terms of their local tangent vectors (velocities),

$$\frac{dx}{d\alpha} = a(t, x), \quad \frac{dt}{d\alpha} = b(t, x)\,. \tag{A2}$$

Integrating this equations yields a whole family of characteristic curves which is parameterized by the starting position x_0 of the curves at $t = 0$ so that $x(\alpha = 0) = x_0$ and $t(\alpha = 0) = 0$. This ensures that from each position of the line $t = 0$ exactly one characteristic curve originates, providing the trajectory along which the initial data $f_0(x)$ can be propagated in time. In order to see why the definition of Eq. (A2) is useful we compute the change of f along the characteristic curves, yielding

$$\frac{df}{d\alpha} + c(t,x)\, f = 0\,. \tag{A3}$$

The crucial observation is that the latter equation is just an *ordinary* differential equation, which is valid along the characteristic curves. To find the final solution $f(t,x)$ to Eq. (A1) one proceeds as follows. First, one solves Eq. (A2) to obtain the relation between (t,x) and (α, x_0). Second, the ordinary differential Eq. (A3) is solved with the initial condition $f(\alpha = 0) = f_0(x_0)$ which provides the solution $f(\alpha, x_0)$. Finally, the parameters α and x_0 are computed for a given coordinate (t,x) to get the solution $f(t,x)$ in the original coordinate frame.

Having outlined the general idea behind the method of characteristics, we can go ahead and turn to the case of two non-linear hyperbolic equations for two functions. We will consider a general system of the form

$$L_1 \;=\; A_1\,\partial_x R + B_1\,\partial_t R + C_1\,\partial_x Z + D_1\,\partial_t Z + E_1 = 0 \tag{A4a}$$
$$L_2 \;=\; A_2\,\partial_x R + B_2\,\partial_t R + C_2\,\partial_x Z + D_2\,\partial_t Z + E_2 = 0 \tag{A4b}$$

for the functions $R(t,x)$ and $Z(t,x)$, where the coefficients A_1, A_2, B_1, …, are known functions of x, t, R and Z. The type of this system depends on the coefficients. For the hyperbolic case in which we are interested here one needs that $ac - b^2 < 0$ with the functions

$$a = [A,C], \quad 2b = [A,D] + [B,C], \quad c = [B,D]\,, \tag{A5}$$

where $[X,Y] = X_1 Y_2 - X_2 Y_1$.

The goal is again to reduce the above system to a system of ordinary differential equations with respect to new coordinates α, β. Since we have now to deal with two unknown functions $R(t,x)$ and $Z(t,x)$ we start by searching for a linear combination $L = \lambda_1 L_1 + \lambda_2 L_2$ of the differential operators in Eq. (A4) so that the derivatives of R and those of Z combine to derivatives in the same direction. These directions will be the velocity vectors of the characteristic curves and thus determine the new coordinate frame. Let us represent an arbitrary curve in the $x - t$ plane by $[t(\sigma), x(\sigma)]$ with σ denoting the running parameter along the curve — note that σ finally will play the role of α or β. Then the condition that in L both functions R and Z are differentiated in the tangential direction of this curve reads

$$\frac{dx/d\sigma}{dt/d\sigma} = \frac{\lambda_1 A_1 + \lambda_2 A_2}{\lambda_1 B_1 + \lambda_2 B_2} = \frac{\lambda_1 C_1 + \lambda_2 C_2}{\lambda_1 D_1 + \lambda_2 D_2}\,. \tag{A6}$$

Next, we consider the change of the functions R and Z along the curve $[t(\sigma), x(\sigma)]$. It is given by $dR/d\sigma = \partial_x R\, dx/d\sigma + \partial_t R\, dt/d\sigma$ and analogous for Z. Multiplying L with either $dx/d\sigma$ or $dt/d\sigma$ and using the conditions of Eq. (A6) one gets

$$\frac{dx}{d\sigma} L \;=\; (\lambda_1 A_1 + \lambda_2 A_2)\,\frac{dR}{d\sigma} + (\lambda_1 C_1 + \lambda_2 C_2)\,\frac{dZ}{d\sigma} + (\lambda_1 E_1 + \lambda_2 E_2)\,\frac{dx}{d\sigma} \tag{A7a}$$
$$\frac{dt}{d\sigma} L \;=\; (\lambda_1 B_1 + \lambda_2 B_2)\,\frac{dR}{d\sigma} + (\lambda_1 D_1 + \lambda_2 D_2)\,\frac{dZ}{d\sigma} + (\lambda_1 E_1 + \lambda_2 E_2)\,\frac{dt}{d\sigma}\,. \tag{A7b}$$

If the functions R and Z satisfy the system of differential Eqs. (A4) we have $L = 0$, and we obtain the following four homogeneous linear equations for the coefficients λ_1 and λ_2 which result from Eq. (A6) and Eq. (A7),

$$\lambda_1 \left(A_1 \frac{dt}{d\sigma} - B_1 \frac{dx}{d\sigma} \right) + \lambda_2 \left(A_2 \frac{dt}{d\sigma} - B_2 \frac{dx}{d\sigma} \right) \;=\; 0 \tag{A8a}$$
$$\lambda_1 \left(C_1 \frac{dt}{d\sigma} - D_1 \frac{dx}{d\sigma} \right) + \lambda_2 \left(C_2 \frac{dt}{d\sigma} - D_2 \frac{dx}{d\sigma} \right) \;=\; 0 \tag{A8b}$$
$$\lambda_1 \left(A_1 \frac{dR}{d\sigma} + C_1 \frac{dZ}{d\sigma} + E_1 \frac{dx}{d\sigma} \right) + \lambda_2 \left(A_2 \frac{dR}{d\sigma} + C_2 \frac{dZ}{d\sigma} + E_2 \frac{dx}{d\sigma} \right) \;=\; 0 \tag{A8c}$$
$$\lambda_1 \left(B_1 \frac{dR}{d\sigma} + D_1 \frac{dZ}{d\sigma} + E_1 \frac{dt}{d\sigma} \right) + \lambda_2 \left(B_2 \frac{dR}{d\sigma} + D_2 \frac{dZ}{d\sigma} + E_2 \frac{dt}{d\sigma} \right) \;=\; 0\,. \tag{A8d}$$

This system is obviously over-determined. Thus, in order to have a non-trivial solution, the determinant of every pair of rows in the matrix of coefficients of λ_1 and λ_2 has to vanish. The relations following from this conditions are called *characteristic relations*.

In particular, from the first two Eqs. (A8a), (A8b), one obtains the condition

$$a\left(\frac{dt}{d\sigma}\right)^2 - 2b\,\frac{dx}{d\sigma}\frac{dt}{d\sigma} + c\left(\frac{dx}{d\sigma}\right)^2 = 0 \tag{A9}$$

with the coefficients given by Eq. (A5). From this condition it becomes clear why the method of characteristics applies to hyperbolic systems. For those systems we have, as mentioned above, $ac - b^2 < 0$, and Eq.(A9) has two different solutions and thus two different characteristic directions $(dx/d\sigma, dt/d\sigma)$ through each point. In the following we assume, without any restrictions, that $a \neq 0$ so that $dx/d\sigma \neq 0$ and we can introduce the slope

$$\zeta = \frac{dt/d\sigma}{dx/d\sigma}\,. \tag{A10}$$

The two different real solutions of $a\zeta^2 - 2b\zeta + c = 0$ for these so-called characteristic directions will be denoted by ζ_+ and ζ_-, respectively. These characteristic directions are in general functions of t, x, R and Z. Two one-parameter families of characteristic curves follow from the directions by integration of the ordinary differential equations $dt/dx = \zeta_+(x,t,R,Z)$ and $dt/dx = \zeta_-(x,t,R,Z)$. In the following we will denote the families of curves by C_+ and C_-. These two families of curves define a curved coordinate net if the curves are represented as $\alpha(x,t) =$ constant and $\beta(x,t) =$ constant for family C_- and C_+, respectively. The functions $\alpha(x,t)$ and $\beta(x,t)$ are called *characteristic parameters*. The coordinates (t,x) corresponding to a given pair (α,β) can be obtained as follows. Consider a curve $\mathcal{I}$ given by $[x(s),t(s)]$ which has nowhere a characteristic direction as tangential vector. In practice, $\mathcal{I}$ will be usually the line $t = 0$ where the initial data are defined. In addition boundary conditions, e.g., a fixed flux at a given position, can be specified by a curve with $x =$constant. Through the two points $s = \alpha$ and $s = \beta$ on the curve $\mathcal{I}$ one follows the characteristic curve of family C_- and C_+, respectively, up to the point where the two curves intersect. The new coordinates of this intersection point (t,x) are then (α,β). The characteristic parameters α and β can now replace the parameter σ for the curves of family C_+ and C_-, respectively, so that one has $dt/d\alpha = \zeta_+ dx/d\alpha$ and $dt/d\beta = \zeta_- dx/d\beta$.

Next, we have to find equations which determine the evolution of the functions R and Z along the characteristic curves. This can be done by eliminating λ_1 and λ_2 from the Eqs.(A8a) and (A8c). Using $dt/d\sigma = \zeta dx/d\sigma$, where ζ denotes either ζ_+ or ζ_- and σ is either α or β, one obtains

$$T\frac{dR}{d\sigma} + (a\zeta - S)\frac{dZ}{d\sigma} + (K\zeta - H)\frac{dx}{d\sigma} = 0\,, \tag{A11}$$

with the coefficients

$$T = [A,B], \quad S = [B,C], \quad K = [A,E], \quad H = [B,E]\,. \tag{A12}$$

If we apply the latter equation to the curves of C_+ and C_- and combine them with the equations for the characteristic curves, we finally obtain the following four *characteristic equations* which are differential equations for the four functions $x(\alpha,\beta)$, $t(\alpha,\beta)$, $R(\alpha,\beta)$ and $Z(\alpha,\beta)$ and replace the original system of Eq. (A4),

$$\partial_\alpha t - \zeta_+ \partial_\alpha x = 0\,, \tag{A13a}$$
$$\partial_\beta t - \zeta_- \partial_\beta x = 0\,, \tag{A13b}$$
$$T\partial_\alpha R + (a\zeta_+ - S)\partial_\alpha Z + (K\zeta_+ - H)\partial_\alpha x = 0\,, \tag{A13c}$$
$$T\partial_\beta R + (a\zeta_- - S)\partial_\beta Z + (K\zeta_- - H)\partial_\beta x = 0\,. \tag{A13d}$$

All the coefficients in this system are known functions of x, t, R and Z. It can be shown that every solution of this characteristic systems satisfies the original system of Eq. (A4) provided that $\partial_\alpha x \partial_\beta t - \partial_\beta x \partial_\alpha t = (\zeta_- - \zeta_+)\partial_\alpha x \partial_\beta x$ is non-zero. With the derivation of Eq. (A13) we reached our initial objective to reduce the partial differential equations to a form which resembles that of ordinary differential equations along certain curves. This can be seen from the fact that each equation contains derivatives with respect to only one of the coordinates α and β. Moreover, the system has to the convenient property that the coefficients do not dependent on the independent variables α and β.

Now we are in the position to outline the strategy for solving an initial value problem for the system of Eq. (A4). Let us assume that the initial values of the functions R and Z are given on the line $t = 0$ by $R_0(x)$ and $Z_0(x)$, and that this line has no characteristic directions. This line corresponds then to the curve $\mathcal{I}$ introduced above. We may

consider this curve as the image of the characteristic parameters obeying the relation $\alpha + \beta = 0$. Then we have to solve the system of Eq. (A13) with the initial conditions

$$t(\alpha, -\alpha) = 0, \quad x(\alpha, -\alpha) = \alpha, \quad R(\alpha, -\alpha) = R_0(\alpha), \quad Z(\alpha, -\alpha) = Z_0(\alpha)\,. \tag{A14}$$

Due to the particular simple structure of the system of Eq.(A13), this problem can be treated as completely as the initial value problem for ordinary differential equations. It is this formulation of the non-linear hyperbolic flow problem which we used throughout the paper to solve the partial differential equations exactly. Finally, we note that this method can be generalized to an arbitrary number n of equations. Then the system will have n characteristic directions ζ_n and correspondingly n different families of characteristic curves. However, the n resulting characteristic parameters can no longer be interpreted as a new coordinate frame since there are only the two coordinates t and x.

APPENDIX B: DERIVATION OF THE SHOCK CONDITION

In this appendix we first review the mechanism for the generation of shocks and their mathematical definition. Then we provide for model $\mathcal{P}$ the details of the calculations for the shock existence criterion and the time and position of the shock. For model $\mathcal{L}$ shocks are always generated, and we derive the simple result of Eq. (45) for the shock time. In Appendix A we have assumed that the characteristic curves of one family (either C_+ or C_-) do not intersect. Only if this is true there is a well defined mapping between the original coordinates (t, x) and the characteristic parameters (α, β). However, depending on the initial data at zero time, it is possible that characteristics of the same family intersect at a finite time. Beyond this shock time the system of partial differential equations fails to have a single valued solution but only multi-valued solutions or even no solution at all exists at later times. The points of intersection of characteristic curves are enclosed by an envelope, cf. Fig.5. The earliest time where a shock appears is the position of the cusp of this envelope. Technically, the envelope is defined by the condition that for every position on the envelope there exists a characteristic curve that touches the envelope at the position so that both curves have the same tangential direction. If we represent the envelope as $[t_e(\alpha), x_e(\alpha)]$ where α is used as the parameter changing along the envelope then the conditions read

$$x_\alpha(t_e(\alpha)) = x_e(\alpha), \quad \partial_\alpha x_\alpha(t)|_{t=t_e(\alpha)} = 0. \tag{B1}$$

where $x_\alpha(t)$ is the trajectory of the characteristic curve along which α is constant. The second condition follows from the requirement that the tangent vector $[1, \partial_t x_\alpha(t)]$ of the curve $x_\alpha(t)$ is parallel to the tangent $[dt_e(\alpha)/d\alpha, dx_e(\alpha)/d\alpha]$ of the envelope. To see this, one takes the derivative of the first condition of Eq. (B1) with respect to α so that one obtains

$$\frac{dx_e(\alpha)}{d\alpha} = \partial_t x_\alpha(t)\frac{dt_e(\alpha)}{d\alpha} + \partial_\alpha x_\alpha(t)|_{t=t_e(\alpha)}\,. \tag{B2}$$

The collinearity of the two tangent vectors requires then the last term on the rhs of Eq. (B2) to vanish. Notice that in model $\mathcal{P}$ the characteristic curves along which β is constant are straight lines, and thus they can never produce a shock.

In the following we focus on the initial profile $R_0(x)$ given by Eq. (9) which allows for an explicit calculation of the envelope and the condition for shocks. For this profile it is useful to consider three different sectors in the $t - x$ plane, see Fig. 4. Using the above conditions, one obtains for the envelope in sector (II) the result

$$t_e(\alpha) = \frac{1}{m - 1/\delta} \ln\left[-\frac{m}{h'(\alpha)} - \frac{1}{h(\alpha)}\right] \tag{B3a}$$

$$x_e(\alpha) = \frac{1}{m - 1/\delta}\left[h(\alpha)e^{(m-1/\delta)t_e(\alpha)} + \ln\left(\frac{h(\alpha)}{r_0}\right) + m\alpha - r_0\right], \tag{B3b}$$

where the function $h(\alpha)$ is given by Eq. (18). In sectors (I) and (III) the conditions of Eq. (B1) cannot be satisfied and thus the characteristics in these sectors never form an envelop. This can be seen as follows. In sector (I), the characteristics along which α is constant are given by

$$x_\alpha(t) = \alpha + R_0(\alpha)\frac{e^{(m+1/\delta)t} - 1}{m + 1/\delta}\,. \tag{B4}$$

Using this expression, the second condition of Eq. (B1) becomes

$$0 = 1 + \frac{R_0'(\alpha)}{m + 1/\delta}\left[e^{(m+1/\delta)t} - 1\right]. \tag{B5}$$

For $m+1/\delta > 0$, the term added to one on the rhs is positive for $t > 0$ since $R_0'(\alpha) > 0$ for negative α in sector (I). In the opposite case $m+1/\delta < 0$, the same argument applies since the expression in the square brackets in now negative for $t > 0$. This shows that the rhs is always larger than one, and the condition is never fulfilled. In sector (III) we use a different argument to show that no α=constant characteristics, which originate from positive x at $t = 0$, form an envelope. From the characteristics in sector (III), the conditions of Eq. (B1) are formally fulfilled by the expression

$$t_e(\alpha) = \frac{1}{m-1/\delta} \ln\left[1 - \frac{m-1/\delta}{R_0'(\alpha)}\right] \tag{B6a}$$

$$x_e(\alpha) = \alpha - \frac{R_0(\alpha)}{R_0'(\alpha)} \tag{B6b}$$

for the envelope. However, it remains to be checked that this curve is indeed located in sector (III), i.e., if its coordinates are larger than the boundary between sectors (II) and (III), cf. Eq. (14b), which yields

$$x_e(\alpha) > \frac{r_0}{m-1/\delta}\left[e^{(m-1/\delta)t_e(\alpha)} - 1\right]. \tag{B7}$$

Using the definition of $R_0(x)$, cf. Eq. (9), and the relation $R_0'(\alpha) = -(1/\delta)R_0(\alpha)/(1+R_0(\alpha))$, the latter condition turns out to be equivalent to

$$\ln\left(\frac{R_0(\alpha)}{r_0}\right) + \frac{r_0}{R_0(\alpha)} < 1. \tag{B8}$$

Since $R_0(\alpha)/r_0 < 1$ for $\alpha \neq 0$, this condition is in fact never fulfilled which proves the absence of shocks in sector (III).

Knowing that shocks, i.e., the cusp of the envelope, can occur only in sector (II) we can try to obtain the condition for shock generation and the time and position of the shock. First consider a negative slope $m < 0$. Then the characteristics in sector (II) saturate at large times,

$$\lim_{t\to\infty} x_\alpha(t) = \frac{r_0}{1/\delta - m}\left[1 - \frac{m}{r_0}\alpha - \frac{1}{r_0}\ln\left(\frac{h(\alpha)}{r_0}\right)\right]. \tag{B9}$$

Since $h(\alpha)$ is a monotonously decreasing function for negative α, the expression in the square brackets is monotonously increasing in α. Thus the characteristics retain the original order for all times, i.e., they never intersect. The situation is more complicated for positive m. Let us assume that there exists a finite value m_c so that only for $m > m_c$ shocks are produced. Then, one expects that at $m = m_c$ the time t_s for the shock appearance tends to infinity in order to have no shocks at finite times for $m < m_c$. Since the shock position (t_s, x_s) is the cusp of the envelope, we have to analyze the large time behavior of the envelope of Eq. (B3). We start with the assumption that the critical value $m_c < 1/\delta$, and, in fact, at the end we will confirm this assumption. For $m < 1/\delta$ one has the asymptotic behavior $t_e(\alpha) \sim -\alpha$, and thus we consider large negative values for α in the following. The shock time is given by the minimal time of the envelope $t_s = t_e(\alpha_m)$ with α_m the parameter at the minimum, i.e., $dt_e(\alpha)/d\alpha = 0$ for $\alpha = \alpha_m$. Then close to the critical slope m_c, we expect that $\alpha_m \to -\infty$. For large negative α, the function $h(\alpha)$ of Eq. (18) has the asymptotic form

$$h(\alpha) \simeq r_0^{1-\nu}(-m\alpha)^\nu e^{r_0(1-\nu)(1+\alpha/\delta)} \tag{B10}$$

with $\nu = (2/\delta)/(m+1/\delta)$. Using this expansion in Eq. (B3) the condition $dt_e(\alpha)/d\alpha = 0$ becomes at asymptotically large α independent of α and assumes the simple form

$$m = \frac{\nu - 1}{\delta}. \tag{B11}$$

Since we assumed that the shock time $t_s \to \infty$, this condition has to be regarded as an equation for the critical slope $m = m_c$. Since ν depends on m the equation is quadratic in m, and it has one negative solution which we have to discard and the other solution gives the critical slope beyond which shocks occur,

$$m_c = \frac{\sqrt{2}-1}{\delta}. \tag{B12}$$

This is the result given in Eq. (19). The behavior of t_s close to $m = m_c$ can be obtained by computing the leading correction to the (constant) asymptotic expression for $dt_e(\alpha)/d\alpha$. We find a correction $\sim 1/\alpha$ which in turn yields the leading order of α_m close to m_c,

$$\alpha_m = -\frac{1}{\sqrt{2}}\frac{1}{m - m_c}. \tag{B13}$$

Since at large negative α the time coordinate of the envelope behaves as $t_e(\alpha) \sim -\alpha$ and $t_s = t_e(\alpha_m)$, we obtain the following power law for the shock time close to criticality,

$$t_s \sim \frac{1}{m - m_c}\,, \tag{B14}$$

as given by Eq. (20). The precise time t_s and position x_s of the shock is given for m sufficiently close to m_c by the envelope of Eq. (B3) at $\alpha = \alpha_m$ of Eq. (B13). At larger m the coordinates (t_s, x_s) are difficult to compute. However, at sufficiently large m closed formulas can be obtained. The reason for this is that for m larger than some threshold the minimum of $t_e(\alpha)$ is always at $\alpha_m = 0$, i.e., the shock is located on the boundary between sectors (II) and (III). To see this, we expand the envelope of Eq. (B3) now around small negative α. This gives

$$t_e(\alpha) \;=\; \frac{1}{m - 1/\delta} \ln\left(\frac{m\delta(1+r_0) - 1}{r_0}\right) + \frac{1 - 2r_0\delta m}{(1+r_0)(\delta m(1+r_0) - 1)}\,\alpha + \mathcal{O}(\alpha^2) \tag{B15a}$$

$$x_e(\alpha) \;=\; r_0\delta\left(1 + \frac{1}{r_0}\right) + \frac{1 - 2r_0\delta m}{1 + r_0}\,\alpha + \mathcal{O}(\alpha^2)\,. \tag{B15b}$$

The minimum of $t_e(\alpha)$ is at $\alpha = 0$ if the coefficient of α in Eq. (B15a) is negative. The denominator of this coefficient has to be positive since otherwise the argument of the logarithm in Eq. (B15a) would be negative. Thus if the slope m fulfills the two conditions $m > 1/(2r_0\delta)$ and $m > 1/(\delta(1+r_0))$ simultaneously then the shock position is given by $(t_s, x_s) = (t_e(\alpha = 0), x_e(\alpha = 0))$. As mentioned already in Sec. III A for $r_0 < 1$ the first condition is relevant whereas for $r_0 > 1$ the latter condition dominates. Now one may ask if it is possible that m_c is larger than latter thresholds so that the shock would occur no longer at α_m of Eq. (B13) but at $\alpha_m = 0$, i.e., on the boundary between sectors (II) and (III) at rather small times. In fact, for $r_0 < 1$ the condition $m_c > 1/(2r_0\delta)$ is never fulfilled so that the minimum remains at α_m of Eq. (B13). For $r_0 > 1$ the condition $m_c > 1/(\delta(1+r_0))$ leads to $r_0 > \sqrt{2}$. In the latter case the shock occurs always at $\alpha_m = 0$ and the new critical slope is given by $1/(\delta(1+r_0))$. However, it should kept in mind that the width of the perturbation $R_0(x)$ of Eq. (9) is proportional to δ only for $r_0 \lesssim 1$. For larger $r_0 \gtrsim 1$ the width is proportional to $r_0\delta$. From the first term $x_s = x_e(\alpha = 0)$ in Eq.(B15b) we thus conclude that the shock occurs at the uphill end of the avalanche with the shock position approximately given by the uphill end of the perturbation at $t = 0$.

Finally, we study the generation of shocks for model $\mathcal{L}$. We do this by using an approach which is more adapted to the special structure of the solution of this model. We do not use directly the definition of Eq. (B1) but look for a discontinuity in the profile $R(t, x)$ as a function of x. If there is a jump in $R(t, x)$ at some position x then a shock is generated and the earliest time where this happens if the shock time t_s. We start from Eq. (42) which gives

$$R(\alpha, \beta) = R_0(\alpha) + mt\,. \tag{B16}$$

By taking the derivative with respect to x, one obtains

$$\partial_x R = R_0'(\alpha)\,\partial_x\alpha\,. \tag{B17}$$

Since $R_0'(x)$ remains finite, we have to search for a divergence in $\partial_x\alpha$. The characteristic parameter $\alpha(t, x)$ can be obtained from Eqs. (41c) and (42) which yield

$$\alpha(t, x) = x + \frac{m}{2}t^2 + R_0(\alpha)\,t\,, \tag{B18}$$

which leads to

$$\partial_x\alpha = \frac{1}{1 - R_0'(\alpha)t}\,. \tag{B19}$$

Since there is always an interval of values for α where a localized $R_0(x)$ has a positive derivative, shocks are generated *always*. The time scale t_s for the occurrence of the shock is the earliest time where $\partial_x\alpha$ diverges, i.e., it is given by the maximal slope of the initial perturbation,

$$t_s = \frac{1}{\max R_0'(x)}\,, \tag{B20}$$

which is Eq. (45). The position x_s of the shock follows from Eq. (B18). For the Gaussian perturbation $R_0(x) = r_0 \exp(-x^2/\delta^2)$ discussed in Section IV A one has $t_s = \sqrt{e/2}\,\delta/r_0$ and the position is given by

$$x_s = -\sqrt{2}\delta - \frac{e}{4}\left(\frac{\delta}{r_0}\right)^2 m\,. \tag{B21}$$

Note that the shock occurs at the downhill front of the avalanche as opposed to the uphill position in model $\mathcal{P}$.

---

[1] GdR Milieux Divisés,
On dense granular flows,
to appear in Eur. Phys. J. E, `cond-mat/0312502`.

[2] I.S. Aronson and L.S. Tsimring,
Continuum description of avalanches in granular media,
Phys. Rev. E **64**, 020301(R) (2001).

[3] J. Rajchenbach,
Development of grain avalanches,
Phys. Rev. Lett. **89**, 074301 (2002).

[4] L. D. Landau, E. M. Lifshitz,
Course of theoretical physics,
Vol. 6 Fluid Mechanics (Pergamon Press) Oxford 1959.

[5] S.B. Savage and K. Hutter,
The motion of a finite mass of granular material down a rough incline,
J. Fluid Mech. **199**, 177 (1989).

[6] O.Pouliquen,
On the shape of granular fronts down rough inclined planes,
Phys. Fluids **11**, 1956 (1999).

[7] O. Pouliquen and Y. Forterre,
Friction law for dense granular flows: application to the motion of a mass down a rough inclined plane,
J. Fluid Mech. **453**, 133 (2002).

[8] E. Lajeunesse, A. Mangeney-Castelnau and J.-P. Vilotte,
Spreading of a granular mass on an horizontal plane,
Phys. Fluids **16**, 2371 (2004).

[9] A. Mangeney-Castelnau, F. Bouchut, E. Lajeunesse, A. Aubertin, J.-P. Vilotte and M. Pirulli,
On the use of Saint-Venant equations for simulating the spreading of a granular mass,
to appear in J. Geol. Resch.

[10] A. Daerr and S. Douady,
Two types of avalanche behaviour in granular media,
Nature **399**, 241 (1999).

[11] A. Daerr,
Dynamical equilibrium of avalanches on a rough plane,
Phys. Fluids **13**, 2115 (2001).

[12] S. Douady, B. Andreotti and A. Daerr,
On granular surface flow equations,
Eur. Phys. J. B **11**, 131 (1999).

[13] T.S. Komatsu, S. Inagaki, N. Nakagawa and S. Nasuno,
Creep motion in a granular pile exhibiting steady surface flow,
Phys. Rev. Lett. **86**, 1757 (2002).

[14] J.-P. Bouchaud, M.E. Cates, J.R. Prakash and S.F. Edwards,
A model for the dynamics of sandpile surfaces,
J. Phys. I (France) **4**, 1383 (1994).

[15] T. Emig, P. Claudin and J.-P. Bouchaud,
Exact solutions of a model for granular avalanches,
Europhys. Lett. **50**, 594 (2000).

[16] A. Mangeney, P. Heinrich and R. Roche,
Analytical Solution for Testing Debris Avalanche Numerical Models,
Pure Appl. Geophys. **157**, 1081 (2000).

[17] F. da Cruz,
Friction and jamming in granular flows,
PhD Thesis (2004), École Nationale des Ponts et Chaussées, Marne la Vallée, France.

[18] L.E. Silbert, D. Ertaş, G.S. Grest, T.C. Halsey, D. Levine, and S.J. Plimpton,
Granular flow down an inclined plane: Bagnold scaling and rheology,
Phys. Rev. E **64**, 051302 (2001).

[19] L. Quartier, B. Andreotti, S. Douady and A. Daerr,
Dynamics of a grain on a sandpile model,
Phys. Rev. E **62**, pp 8299 (2000).

[20] D. Bonamy, F. Daviaud, and L. Laurent,

Experimental study of granular surface flows via a fast camera: A continuous description,
Phys. Fluids **14**, 1666 (2002).

[21] N. Taberlet, P. Richard, A. Valance, W. Losert, J.M. Pasini, J.T. Jenkins, and R. Delannay,
Superstable granular heap in a thin channel,
Phys. Rev. Lett. **91**, 264301 (2003).

[22] D.V. Khakhar, A.V. Orpe and J.M. Ottino,
Surface Granular flows: Two Related Examples,
Preprint, `cond-mat/0406602`.

[23] D.V. Khakhar, J.J. McCarthy, T. Shinbrot and J.M. Ottino,
Transverse flow and mixing of granular materials in a rotating cylinder,
Phys. Fluids **9**, 31 (1997).

[24] B. Andreotti and S. Douady,
Selection of velocity profile and flow depth in granular flows,
Phys. Rev. E **63**, 031305 (2001).

[25] D. Bonamy, F. Daviaud, L. Laurent, M. Bonetti, and J.-P. Bouchaud,
Multiscale Clustering in Granular Surface Flows,
Phys. Rev. Lett. **89**, 034301 (2002).

[26] A. Aradian, E. Raphaël and P.-G. de Gennes,
Thick surface flows of granular materials: effet of the velocity profile on the avalanche amplitude,
Phys. Rev. E **60**, 2009 (1999).

[27] D.V. Khakhar, A.V. Orpe, P. Andresé and J.M. Ottino,
Surface flow of granular materials: model and experiments in heap formation,
J. Fluid Mech. **441**, 255 (2001).

[28] Lambert's function $W(x)$ is defined by $W(x)e^{W(x)} = x$. For very large values of x, one has $W(x) \sim \ln x - \ln\ln x$. In contrast, $W(x) \sim x - x^2$ for $x \ll 1$. Its derivative can simply expressed by $W'(x) = \frac{W(x)}{x[1+W(x)]}$, see, e.g., R. M. Corless, G. H. Gonnet, D. E. G. Hare, D. J. Jeffrey, D. E. Knuth, Maple Share Library.

[29] T. Boutreux, E. Raphaël and P.-G. de Gennes,
Surface flows of granular materials: A modified picture for thick avalanches,
Phys. Rev. E **58**, 4692 (1988).

[30] S. Douady, B. Andreotti, P. Cladé and A. Daerr,
The four avalanche fronts: a test case for granular surface flow modeling,
Advances in Complex Systems **4**, 509 (2001).

[31] R. Courant, K. O. Friedrichs,
Supersonic Flow and Shock Waves,
Interscience Pub., New York (1956).